

Shockwave Consolidation of Nano Silver Powder into Bulk Nano Structured Silver

By

Li Zhang

Department of Mining, Metals and Materials Engineering

McGill University

Montreal, Canada

August, 2007

A thesis submitted to McGill University in partial fulfilment of the requirements of the degree of Master of Engineering



© Li Zhang, 2007



Library and
Archives Canada

Published Heritage
Branch

395 Wellington Street
Ottawa ON K1A 0N4
Canada

Bibliothèque et
Archives Canada

Direction du
Patrimoine de l'édition

395, rue Wellington
Ottawa ON K1A 0N4
Canada

Your file Votre référence
ISBN: 978-0-494-38498-5
Our file Notre référence
ISBN: 978-0-494-38498-5

NOTICE:

The author has granted a non-exclusive license allowing Library and Archives Canada to reproduce, publish, archive, preserve, conserve, communicate to the public by telecommunication or on the Internet, loan, distribute and sell theses worldwide, for commercial or non-commercial purposes, in microform, paper, electronic and/or any other formats.

The author retains copyright ownership and moral rights in this thesis. Neither the thesis nor substantial extracts from it may be printed or otherwise reproduced without the author's permission.

AVIS:

L'auteur a accordé une licence non exclusive permettant à la Bibliothèque et Archives Canada de reproduire, publier, archiver, sauvegarder, conserver, transmettre au public par télécommunication ou par l'Internet, prêter, distribuer et vendre des thèses partout dans le monde, à des fins commerciales ou autres, sur support microforme, papier, électronique et/ou autres formats.

L'auteur conserve la propriété du droit d'auteur et des droits moraux qui protège cette thèse. Ni la thèse ni des extraits substantiels de celle-ci ne doivent être imprimés ou autrement reproduits sans son autorisation.

In compliance with the Canadian Privacy Act some supporting forms may have been removed from this thesis.

Conformément à la loi canadienne sur la protection de la vie privée, quelques formulaires secondaires ont été enlevés de cette thèse.

While these forms may be included in the document page count, their removal does not represent any loss of content from the thesis.

Bien que ces formulaires aient inclus dans la pagination, il n'y aura aucun contenu manquant.


Canada

ABSTRACT

Bulk nanostructured silver components were fabricated from nano-sized powder using a shockwave consolidation technique. The grain size evolution during compaction, the mechanical properties of the bulk components, and the effect of surface finish on the mechanical behavior were studied. X-Ray diffraction, transmission electron microscopy (TEM), atomic force microscopy (AFM), microhardness, compression testing and shear punch testing at room temperature were used to characterize the materials. Upon consolidation, the average grain size calculated from image analysis of the TEM micrographs was 49 ± 22 nm, showing the feasibility of maintaining a nanostructure upon dynamic consolidation. The hardness of the bulk nanostructured components was constant across the diameter with an average of 83 ± 1 HV. Compression results showed strength about 390 ± 10 MPa and ductility of $23\pm 2\%$, which is well above strength level obtainable from strain hardened Ag components. The AFM results show that samples possessing a surface roughness of 267 nm exhibited a brittle behavior and a reduction in strength of 35% when compared to the smoother surfaces. Dimples were observed for the samples exhibiting plasticity, while an intergranular pattern was identified for the brittle materials. Fracture toughness of $0.2 \text{ MPa}\sqrt{\text{m}}$ was calculated, which confirms the strong relationship between fracture toughness and defects observed in nanomaterials.

RESUME

Des pièces massives d'argent nanostructurées ont été fabriquées à partir de poudres nanométriques à l'aide d'une technique de consolidation par ondes de choc. L'évolution de la taille des grains pendant la compaction, les propriétés mécaniques des pièces massives ainsi que l'effet du fini de surface sur le comportement mécanique ont été étudiés. La diffraction par rayons-X, la microscopie électronique à transmission (MET), la microscopie à force atomique (AFM), la microdureté, les essais en compression ainsi que le poinçon de cisaillement à température ambiante ont été les outils utilisés pour la caractérisation de ces matériaux. Après la consolidation, la taille moyenne des grains calculée à partir d'analyses d'images provenant du MET était de 49 ± 22 nm, démontrant la possibilité de maintenir la nanostructure des poudres après une consolidation dynamique. La dureté des pièces nanostructurées était constante sur tout le diamètre avec une valeur moyenne de 83 ± 1 HV. Les résultats en compression ont démontré une résistance mécanique d'environ 390 ± 10 Mpa et une ductilité de $23 \pm 2\%$, ce qui est supérieur au niveau atteignable avec des pièces d'Ag écrouies. Il a été démontré à partir des résultats d'échantillons analysés à l'AFM que ceux qui possèdent une rugosité de 267 nm ont un comportement fragile ainsi qu'une réduction de 35% de leur résistance mécanique par rapport aux échantillons ayant une surface plus lisse. Un faciès de rupture ductile a été observé sur les échantillons déformés

plastiquement alors qu'une rupture intergranulaire a été observé sur les matériaux fragiles. Une ténacité de $0.2 \text{ MPa}\sqrt{\text{m}}$ a été calculée, ce qui confirme la relation évidente entre les défauts observés dans les nanomatériaux et leur ténacité.

CONTRIBUTIONS OF AUTHORS

This thesis has been written as a series of manuscripts. The following are the co-authored manuscripts that have been submitted in order to complete this thesis.

The candidate is the primary author of all manuscripts. All of the manuscripts are co-authored by Professor Mathieu Brochu in his capacity as research supervisor. In addition, the manuscripts have all been co-authored by Dr. Abdelbaset M Elwazri in his capacity as post-doctoral fellow. Mr. Tony Zimmerly has co-authored the manuscripts related to the blast experiments, as he acted in a supervisory capacity while those tests were conducted. All of the consolidation experiments were conducted by Professor Mathieu Brochu, and the characterization experiments were operated by the candidate.

ACKNOWLEDGEMENTS

My first thanks are given to my supervisor, Professor Mathieu Brochu, for his guidance and support throughout the project, as well as for all his efforts and desire to help me improve in every aspect. He has been encouraging and a source of inspiration.

I would like to thank the Natural Sciences and Engineering Research Council of Canada (NSERC) and McGill University for funding this project, and for supporting me with graduate fellowships. Also, I am grateful to the Energetic Materials Research and Testing Center (EMRTC) for allowing access to their sites.

I would also like to express my thanks to all of the personnel in the department, for your support and friendship. Special thanks to Dr. Abdelbaset Elwazri for his help with experiments and for our valuable discussions. My appreciation also goes to my teammates and friends: Abdulaziz, Sean, Umugaba, Yaneth, Ramona, Graeme, Per, Lihong, Xin, Xinran, Lan, Camille, and everybody else not listed here. All of you have filled these two years with friendship, fun, and learning and you have made my stay at McGill University memorable.

My sincerest gratitude and appreciation are given to my family, in particular, my parents and my sister for their unconditional love, continuous support and infinite encouragement. I could not be in this place without their confidence and assistance. I would like to dedicate to them this work to show my endless love.

TABLE OF CONTENTS

| | |
|--|-----|
| ABSTRACT | i |
| RESUME..... | ii |
| CONTRIBUTIONS OF AUTHORS..... | iv |
| ACKNOWLEDGEMENTS..... | v |
| TABLE OF CONTENTS..... | vii |
| LIST OF FIGURES | x |
| LIST OF TABLES | xiv |
| CHAPTER 1 INTRODUCTION | 1 |
| References..... | 7 |
| CHAPTER 2 STRUCTURE & OBJECTIVES OF THESIS..... | 8 |
| CHAPTER 3 REVIEW OF BULK NANOMATERIALS | 9 |
| 3.1. Processing of Bulk Nanomaterials | 9 |
| 3.1.1. Electrodeposition | 10 |
| 3.1.2. Severe Plastic Deformation (SPD)..... | 12 |
| 3.1.3. Mechanical Milling | 13 |
| 3.1.4. Crystallization of Amorphous Solids | 15 |
| 3.1.5. Shock Consolidation | 16 |
| 3.2. Properties of Bulk Nanomaterials..... | 24 |
| 3.2.1. Elastic Properties..... | 25 |
| 3.2.2. Hardness and Strength..... | 27 |

| | |
|--|-----------|
| 3.2.3. Ductility and Toughness | 30 |
| 3.3. References..... | 35 |
| CHAPTER 4 FABRICATION OF BULK NANOSTRUCTURED SILVER MATERIAL FROM NANOPOWDERS USING SHOCKWAVE CONSOLIDATION TECHNIQUE | |
| 43 | |
| 4.1. Introduction | 43 |
| 4.2. Experimental procedures | 45 |
| 4.2.1 Starting Materials..... | 45 |
| 4.2.2 Consolidation Process | 46 |
| 4.2.3 Characterization of Consolidated Specimens | 46 |
| 4.2.3.1 Density | 47 |
| 4.2.3.2 Microstructure Analysis | 47 |
| 4.2.3.3 Hardness Testing | 48 |
| 4.2.3.4 Compression Testing | 48 |
| 4.3. Results | 48 |
| 4.3.1 Starting Materials..... | 48 |
| 4.3.2 Macrostructure of Bars | 49 |
| 4.3.3 Density..... | 50 |
| 4.3.4 X-ray Diffraction..... | 50 |
| 4.3.5 Microstructure | 51 |
| 4.3.6 Hardness | 53 |
| 4.3.7 Compression Testing..... | 55 |
| 4.4. Discussion | 57 |
| 4.5. References..... | 63 |
| CHAPTER 5 THE INFLUENCE OF SURFACE ROUGHNESS ON STRENGTH AND DUCTILITY OF SHOCKWAVE CONSOLIDATED BULK NANOSTRUCTURED SILVER | |
| 65 | |
| 5.1. Introduction | 65 |
| 5.2. Experimental procedures | 67 |

| | |
|---|-----------|
| 5.3. Results and Discussion..... | 69 |
| 5.3.1. Microstructure | 69 |
| 5.3.2. AFM..... | 70 |
| 5.3.3. Shear Punch Testing | 72 |
| 5.3.4. SEM of Fracture Surface | 75 |
| 5.4. References..... | 77 |
| CHAPTER 6 GENERAL DISCUSSION | 79 |
| CHAPTER 7 SUMMARY | 84 |

LIST OF FIGURES

| | |
|--|----|
| Figure 1.1. Classification Scheme for Nanostructured Materials According to Their Chemical Composition and the Dimensionality (Shape) of The Crystallites (Structural Elements) Forming the Nanostructure [1.4]. | 3 |
| Figure 1.2. Two-Dimensional Model of a Nanostructured Material. The Atoms in The Centers of the Crystals are Indicated in Black. The Ones in the Boundary Core Regions are Represented as Open Circles [1.4]. | 4 |
| Figure 1.3. Relation Between the Size of Gold Particles and Melting Point [1.8]. | 4 |
| Figure 1.4. The Effect of Grain Size on Calculated Volume Fractions of Intercrystal Regions and Triple Junctions, Assuming a Grain-Boundary Thickness of 1 nm [1.10]. | 5 |
| Figure 3.1. Pulsed Electrodeposition Set-up for Synthesizing Nanocrystalline Materials [1.11]. | 11 |
| Figure 3.2. Schematic of Severe Plastic Deformation Process with (a) Equal-Channel-Angular Pressing [3.19], (b) High-Pressure Torsion [3.19], and (c) Accumulative Roll-Bonding [3.24]. | 13 |
| Figure 3.3. Mechanical Milling as a Means of Synthesis of Nanostructured Material [3.31]. | 14 |
| Figure 3.4. Schematic Illustrating Various Processes and Their Associated Effects Occurring During Shock Consolidation of Powders [3.50]. | 18 |
| Figure 3.5. Various Modes of Energy Dissipation in Shock Compression of Powders [3.48]. | 19 |
| Figure 3.6. Cracks and Flaws Encountered in Shock Consolidated Cylinders [3.47]. | 21 |

| | |
|---|----|
| Figure 3.7. Pictures of Shockwave Consolidation: (a) Explosive Shockwave Consolidation, (b) Dynamic Magnetic Consolidation, and (c) Gun Impact Consolidation | 22 |
| Figure 3.8. (a) Schematic of the Cetr/Sawaoka 12-Capsule Shock Recovery Fixture Configuration and Explosive Loading System [3.67, 3.68], (b) Cylindrical Modified Double Tube System [3.69]..... | 23 |
| Figure 3.9. (a) Experimental Setup, (b) Symmetrical Explosive Configuration (Longitudinal Sections), and (c) Symmetrical Loading Configuration (Cross-Sections) | 24 |
| Figure 3.10. Young's Modulus as a Function of Porosity for Nanocrystalline Pd and Cu [1.12]. | 25 |
| Figure 3.11. Ratio of The Young's Modulus of Nanocrystalline Materials to Those of Conventional Grain Size Materials as a Function of Grain Size [3.78]. | 26 |
| Figure 3.12. Compiled Yield Stress Versus Grain Size Plot for Cu From Various Sources Ranging from Coarse to Nanograin Size. The Plots Show Different Trends as the Grain Size Falls Below a Critical Size [1.11]. | 29 |
| Figure 3.13. Grain Size Dependence of All Three Contributions to the Total Imposed Strain (Dislocation Mechanism, Grain-Boundary Diffusion and Lattice Diffusion Mechanism) in Cu for the Total Imposed Strain Rates of 10^{-3} S^{-1} [3.83]..... | 29 |
| Figure 3.14. Elongation to Failure in Tension Vs. Grain Size for Some Nanocrystalline Metals and Alloys [3.74]..... | 31 |
| Figure 3.15. Compilation of Yield Stress Versus % Elongation of (a) Nanocrystalline Metals, (b) Ultrafine Grained Metals [3.94]. | 32 |
| Figure 3.16. A Typical Tensile Stress-Strain Curve [3.108] for the Bulk in Situ Consolidated Nanocrystalline Cu Sample, in Comparison with that of a Coarse-Grained Polycrystalline Cu Sample and a Nanocrystalline Cu Sample Prepared by an Inert-Gas Condensation and Compaction Technique [3.110]. | 34 |

| | |
|--|----|
| Figure 4.1. Scanning Electron Micrographs of Two Starting Powders (a) Nano-Ag Powder, and (b) Micro-Ag Powder. | 49 |
| Figure 4.2. Cross Section of the (a) Nano-Ag Specimen, and (b) Micro-Ag Specimen. | 49 |
| Figure 4.3. Collection of X-Ray Diffraction Patterns from the Consolidated Nano-Ag Specimen, Micro-Ag Specimen and the Starting Nano-Ag and Micro-Ag Powders, Respectively. | 51 |
| Figure 4.4. (a) TEM Bright-Field Image of Nano-Ag Specimen Including Selected Area Diffraction Pattern and (b) Grain Size Distribution Measured from TEM Images. | 52 |
| Figure 4.5. Optical Micrograph of Micro-Ag Specimen. | 53 |
| Figure 4.6. Microhardness of Nano-Ag and Micro-Ag Specimens. | 54 |
| Figure 4.7. Stress-Strain Curves of Nano-Ag and Micro-Ag Consolidated Bars. | 55 |
| Figure 4.8. SEM of the Broken Specimens, with Low Magnification (a) Nano -Ag, (b) Micro -Ag, and with High Magnification (c) Nano -Ag, (d) Micro -Ag. | 56 |
| Figure 5.1. TEM Bright-Field Image of Nano-Ag Specimen Including Selected Area Diffraction Pattern. | 70 |
| Figure 5.2. AFM Micrograph of Sample with (a) 600 Grit, (b) 800 Grit and (c) 3 mm Surface Finish. | 71 |
| Figure 5.3. Load-Displacement Curves for Samples Possessing a Roughness Average of 30 nm. | 73 |
| Figure 5.4. Comparison of the Load-Displacement Curves for Samples Possessing Roughness Averages of 267, 30 and 12 nm, Respectively. | 74 |
| Figure 5.5. Comparison of Strength (UTS and Yield Strength (YS)) and EL of Shear Punch Testing as a Function of Surface Finish. | 74 |
| Figure 5.6. SEM of Fracture Surface for (a) 267 nm, (b) 30 nm and (c) 12 nm Surface Finishes, Respectively. | 76 |

| | |
|---|----|
| Figure 6.1. Compilation of Yield Stress Versus % Elongation of Nanocrystalline Metals [3.94]. | 82 |
|---|----|

LIST OF TABLES

| | |
|--|----|
| Table 4.1. Characteristics of the Starting Powders | 45 |
| Table 4.2. Comparison of the Average Grain Size and Lattice Strain of the Consolidated Bars and Starting Powders Specimens..... | 51 |
| Table 4.3. Comparison of the Mechanical Properties of Nano-Ag and Micro-Ag Specimens | 56 |
| Table 5.1. Values of Roughness Average (Ra) and Root Mean Square Average (Rq) as a Function of Surface Finish..... | 71 |

CHAPTER 1

INTRODUCTION

The word “Nano” is derived from the Greek word Dwarf. It means “one billionth”. For example, a nanometer (nm) is one billionth of a meter. To facilitate comparison, a single human hair is about 80,000 nm wide, a red blood cell is approximately 7,000 nm wide and a water molecule is almost 0.3 nm across. The name “nanocrystalline” has become increasingly popular since Herbert Gleiter published the landmark paper *Structure and properties of microcrystalline materials* [1.1] in 1983. In that paper, Gleiter discussed the outstanding possibilities of what he called then “microcrystalline materials”. Eric Drexler popularized the word “nanotechnology” in the 1980's in his book *Engines of Creation: The Coming Era of Nanotechnology* [1.2], which first introduced the basic concepts of nanotechnology to a general audience. Drexler's book described Nanosystems, Molecular Machinery, Manufacturing, and Computation, an applied-physics analysis of advanced productive nanosystems in terms that were widely comprehensible. Since then, a significant portion of the global research efforts in materials science have been redirected to nanomaterials. The U.S. National Nanotechnology Initiative defines “nanomaterial” as anything possessing in at least 1 dimension a length scale smaller than 100 nanometers.

Materials technology research is fundamental to fields such as information processing, environmental protection, living environment safety and energy. Nanomaterials are expected to revolutionize materials technology. To do so, improvements in the functions, properties and characteristics of materials as well as the creation of new functions through controlling materials structure on a super-fine scale need to continue to be developed.

Siegel [1.3] has classified nanostructured materials into four categories according to their dimensionality: 0D – nanoclusters; 1D – multilayers; 2D – nanograined layers; 3D – equiaxed bulk solids.

On the other hand, Figure 1.1 illustrates the classification system for nanostructured materials established by Gleiter [1.4]. Gleiter's taxonomy orders nanostructured materials into families according to composition, morphology, and distribution of the nanocrystalline components. He used three shapes: rods, layers, and equiaxed grains. His classification includes many possible permutations of materials and is quite broad. The boundary regions of the first and second families are indicated in black in Figure 1.1 which emphasizes the different atomic arrangements in the crystallites and their boundaries [1.4].

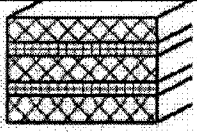
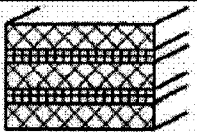
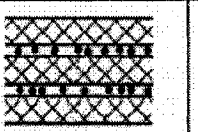
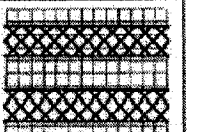
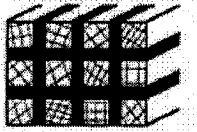
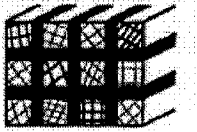
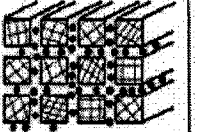
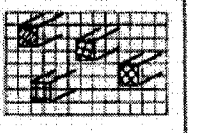
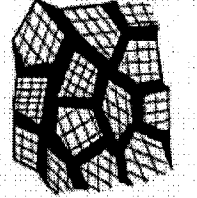
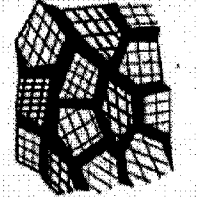
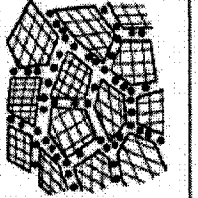
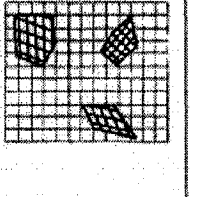
| Chem. comp. of crystallites | Same | Different for different crystallites | Composition of boundaries and crystallites different | Crystallites dispersed in matrix of different composition |
|--------------------------------|--|--|---|--|
| Shape of crystallites | | | | |
| Layer- shaped |  |  |  |  |
| Rod- shaped |  |  |  |  |
| Equiaxed crystallized |  |  |  |  |

Figure 1.1. Classification scheme for nanostructured materials according to their chemical composition and the dimensionality (shape) of the crystallites (structural elements) forming the nanostructure [1.4].

Properties in nanocrystalline materials are altered by the large volume fraction of grain boundaries. This attribute leads to the requirement of new mechanisms to explain the novel mechanical, physical, and chemical properties that occur in nanocrystalline materials [1.5-1.7]. Figure 1.2 shows a schematic depiction of a nanocrystalline material. The grain-boundary atoms are white and are not clearly associated with crystalline symmetry [1.4].

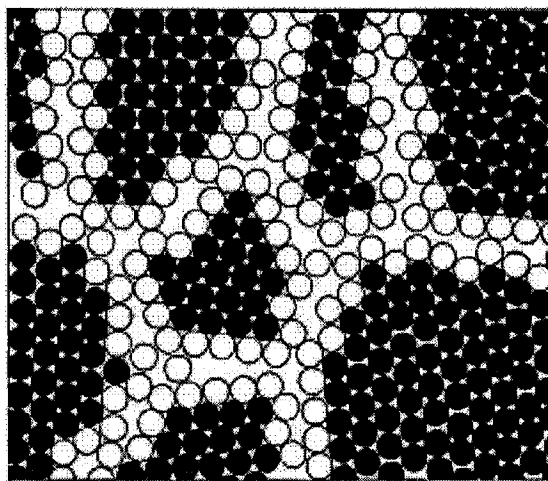


Figure 1.2. Two-dimensional model of a nanostructured material. The atoms in the centers of the crystals are indicated in black. The ones in the boundary core regions are represented as open circles [1.4].

Nanomaterials show very different properties compared to what they exhibit at the macroscale, for instance, the melting point reduces when the particle size becomes small. Figure 1.3 shows the relationship between the size of gold particles and their melting point [1.8]. It can be seen that the melting points of gold particles are obviously affected by the particle size, particularly as it approaches the smaller end of the nanoscale.

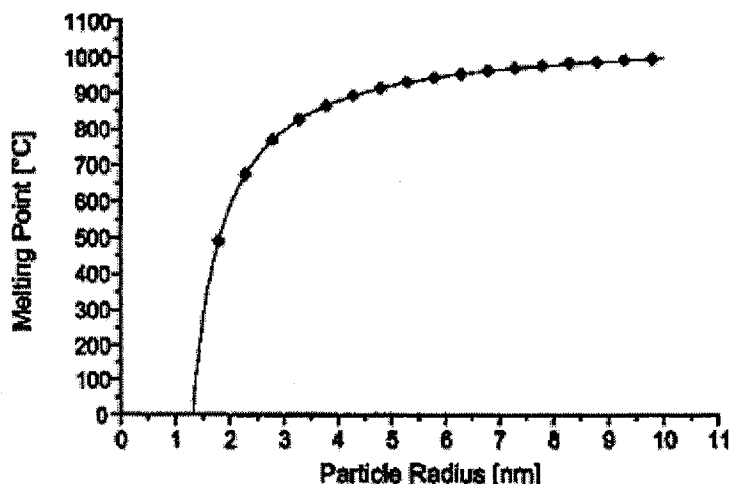


Figure 1.3. Relation between the size of gold particles and melting point [1.8].

Two factors cause the properties of nanomaterials to differ significantly from those of conventional materials: an increased surface area to volume ratio and the quantum effects [1.9]. Firstly, at the nanoscale, an increasing fraction of atoms can be ascribed to the grain boundaries as the grain size decreases. Figure 1.4 shows the change of the volume fraction of intercrystal regions and triple-junctions as a function of grain size [1.10]. Because the nanocrystalline material contains a high density of interfaces, a substantial fraction of atoms lie in the interfaces. The volume fraction of interfaces can be as much as 50% for 5 nm grains, 30% for 10 nm grains, and about 3% for 100 nm grains [1.11]. The atoms on the surface tend to be more reactive than those at the center, which can make materials more chemically reactive and can affect their strength or electrical properties [1.9]. For example, Weertman and coworkers [1.12] observed that nanocrystalline Cu and Pd samples were remarkably stronger than their coarse-grained counterparts.

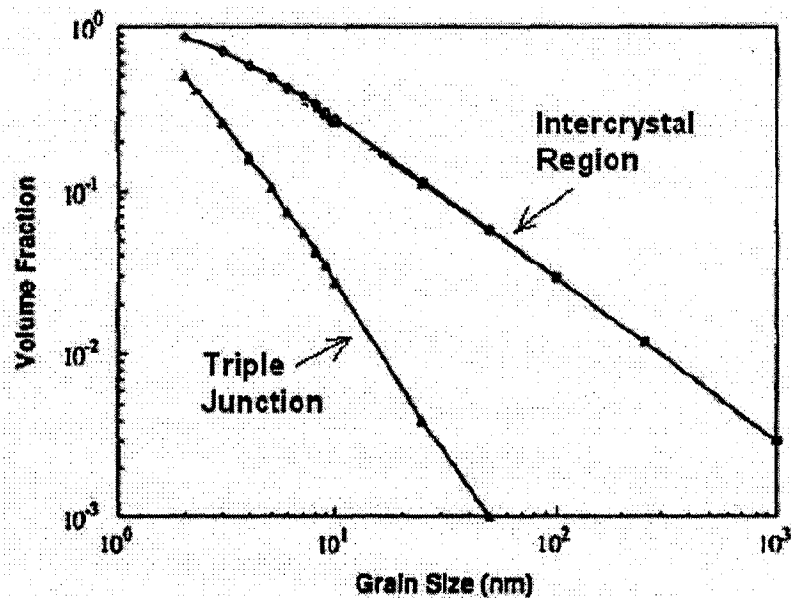


Figure 1.4. The effect of grain size on calculated volume fractions of intercrystal regions and triple junctions, assuming a grain-boundary thickness of 1 nm [1.10].

Secondly, quantum effects can begin to dominate the properties of matter as their size is reduced to the nanoscale. Quantum mechanics are used as a mathematical tool for predicting the behaviors of microscopic particles; quantum effects include wave-particle duality and the Uncertainty Principle. Quantum effects are not noticeable in the macro world, they only become important as one approaches the dimensions of the atom. Nevertheless, their effects are important in all branches of science. Quantum effects can affect the optical, electrical and magnetic behaviour of materials, particularly as the structure or particle size approaches the smaller end of the nanoscale. Much of the fascination with nanotechnology stems from the unique quantum and surface phenomena that matter exhibits at the nanoscale [1.9].

Markets for bulk nanostructured materials appear to exist in every product sector where superior mechanical and physical properties (in particular, high strength, good strength-to-weight ratio, and excellent fatigue life) are critical. The developments of scientists from all over the world have made it attractive to apply nanomaterials in various industries including aerospace, transportation, medical devices, sports products, food and chemical processing, electronics, and conventional defense.

References

- [1.1] Gleiter H., Structure and Properties of Mycrocrystalline Materials. In: Proceedings of Ninth International Vacuum Congress and Fifth International Conference on Solid Surfaces, September 26-30, 1983, Madrid, Spain, S. p. 397 - 405.
- [1.2] Drexler K.E., Engines of Creation: The Coming Era of Nanotechnology. Anchor Books, 1986, ISBN 0385199732.
- [1.3] Siegel R.W., Mechanical properties and deformation behavior of materials having ultrafine microstructures. In: Nastasi M, Parkin DM, Gleiter H, editors; 1993. p. 509.
- [1.4] Gleiter H., Acta Mater 2000;48:1–29.
- [1.5] Cohen J.B., Metall Trans A—Phys Metall Mater Sci 1992;23:2685–97.
- [1.6] Artz E., Acta Mater 1998;46:5611.
- [1.7] Birringer R., Mater Sci Eng A 1989;117:33.
- [1.8] Tjong S.C., et al., Mat Sci & Eng R45, 2004, P.1-88.
- [1.9] Big Picture on Nanoscience, Issue 2 June 2005, Big Picture series, The Wellcome Trust, Freepost, ANG 6754, Ely CB7 4YE
- [1.10] Palumbo G., Thorpe S.J, Aust K.T., Scripta Metall Mater 1990;24:1347–50.
- [1.11] Meyers M.A., Mishra A., Benson D.J., Progress in Materials Science 51, 2006; 427–556
- [1.12] Sanders P.G., Eastman J.A., Weertman J.R., Acta Mater 1997;45:4019-4025.

CHAPTER 2

STRUCTURE & OBJECTIVES OF THESIS

This thesis has been written as a series of manuscripts. The introduction and review sections give background and basic knowledge of bulk nanomaterials. Chapters 4 and 5 contain two paper manuscripts, each of them containing independent experimental procedures, results, discussion, and reference sections. Chapter 4, *Fabrication of Bulk Nanostructured Silver Material from Nanopowders Using Shockwave Consolidation Technique*, focuses on the fabrication and characterization of shock consolidated bulk nanostructured silver components from nano-size powder. In that manuscript, the grain size evolution during compaction and the mechanical properties of the bulk components have been characterized. Micron scale powders were also consolidated for comparison purposes. Chapter 5, *The Influence of Surface Roughness on Strength and Ductility of Shockwave Consolidated Bulk Nanostructured Silver*, focuses on the relationship between room temperature tensile properties, surface roughness and fracture toughness for shock consolidated nanocrystalline Ag samples. Chapters 6 and 7 contain the general discussion and summary, which link the previous chapters.

CHAPTER 3

REVIEW OF BULK NANOMATERIALS

3.1. Processing of Bulk Nanomaterials

Some people talk about a “nanotechnology revolution” as if this was the start of something radically new. However, people have exploited the properties of nanoparticles for centuries. Gold and silver nanoparticles are responsible for some coloured pigments and have been used in stained glass and ceramics since the 10th century [1.9]. Nevertheless, nanomaterials become of interest as a major field in modern materials science in 1981 when Gleiter synthesized nanostructured metals using inert gas condensation (IGC) and in situ consolidation [3.1]. Since it was demonstrated that the synthesis method has a direct and important effect on the mechanical properties of materials, a number of techniques have been developed for producing nanostructured materials, ranging from nanoscale particles to bulk nanostructured materials.

There is one hindrance in the production of nanostructured materials. Unfortunately, while it is relatively easy to synthesize powders and to produce small samples, it is much more difficult to obtain the same materials in forms

large enough for structural applications. The reason for this complication is that the large surface to volume ratio causes nanomaterials to be metastable because the surface energy component of the total free energy of the system cannot be neglected. Therefore, due to the significant disordered grain boundary regions, nanomaterials are thermally unstable and are subjected to a strong driving force for grain growth [3.2, 3.3]. In comparison to their micron-scale counter parts, recrystallisation and grain growth in nanomaterials occurs at a much lower temperature, which can interfere with the processing temperature. The unique properties of nanomaterials are related to fine grain size and the large volume fraction of grain boundaries. Therefore, optimizing the fabrication processes while maintaining the microstructure at a nanometer scale during consolidation is one of the major challenges in fabricating large scale nano-structured components. [3.4].

Various methods for processing bulk nanostructured materials have been developed. Based on the approaches, they can be classified into one-step or two-step methods. The five most common methods used for processing bulk nanostructured materials are summarized below.

3.1.1. Electrodeposition

Electrodeposition has long been used to create coatings (electroplating) and to create free-standing entities (electroforming) [3.5]. Erb et al. [3.6] have studied

the synthesis, structure and properties of nanocrystalline nickel synthesized by pulse electrodeposition. They have demonstrated that conventional or modified electroplating baths and conditions could be used to produce nanocrystalline nickel with a grain size as small as 11 nm. The basic components required to form a cell for electrodeposition are an anode, cathode, electrolyte, and direct-current source. Figure 3.1 shows the pulse electrodeposition sequence schematically.

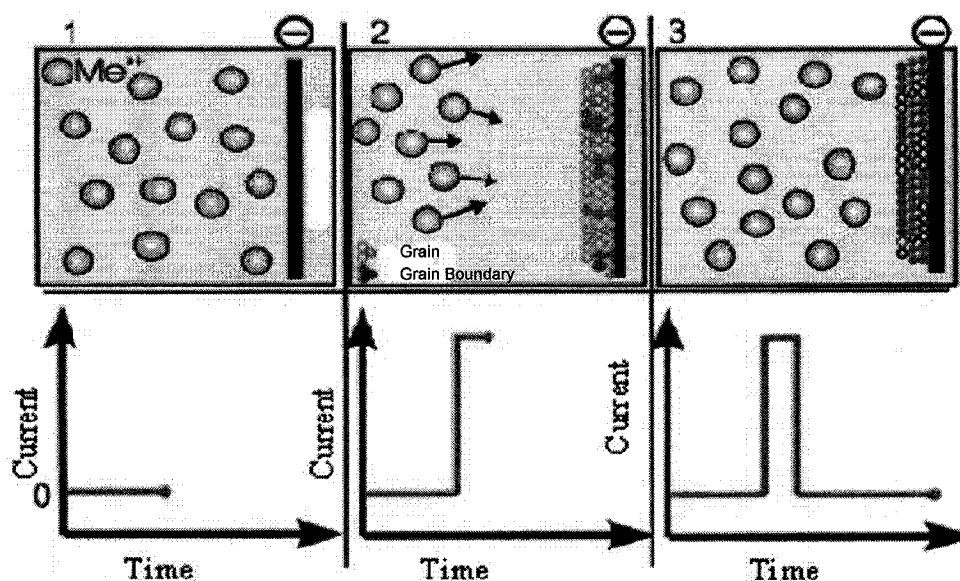


Figure 3.1. Pulsed electrodeposition set-up for synthesizing nanocrystalline materials [1.11].

The main processing parameters for obtaining nanocrystalline materials include the basic composition of the electrolyte, addition of grain nucleators, stress relievers and grain-growth inhibitors, the PH value, the deposition temperature, the current density, and the type of current cycles such as continuous direct-current plating, pulsed direct-current plating, or periodic current-reversal plating [3.6-3.8]. This technique can yield porosity-free finished products that do not require subsequent consolidation processing. Furthermore, this process requires

low capital investment and provides high production rates with few shape and size limitations [1.11].

3.1.2. Severe Plastic Deformation (SPD)

The basic principle behind severe plastic deformation is to impose an extremely high strain deformation on the material of interest such that structural refinement occurs both by the shearing and fracturing of phases and is followed by recrystallization processes [3.9]. The final microstructure is determined by balancing of the rate of work and the rate of recovery. The commonly used severe plastic deformation processes are: (a) equal-channel-angular pressing (ECAP) [3.10-3.17], (b) high-pressure torsion (HPT) [3.18-3.22], and (c) accumulative roll-bonding (ARB) [3.23-3.24]. A schematic of these three processes is shown in Figure 3.2.

In order to process homogeneous structures while minimizing grain size, the major parameters to control include: temperature, strain rate, imposed pressure, lubrication, the intersecting angle (if any) and strain [3.18-3.24]. SPD allows lower contamination in comparison to the powder synthesis approaches, since ingots are the starting materials. SPD is also capable of fabricating bulk materials with no porosities which is a significant advantage over the powder metallurgy route [1.11, 3.9]. The main disadvantage of SPD is the high residual

internal stresses that can result in an unstable microstructure and properties [1.11, 3.9].

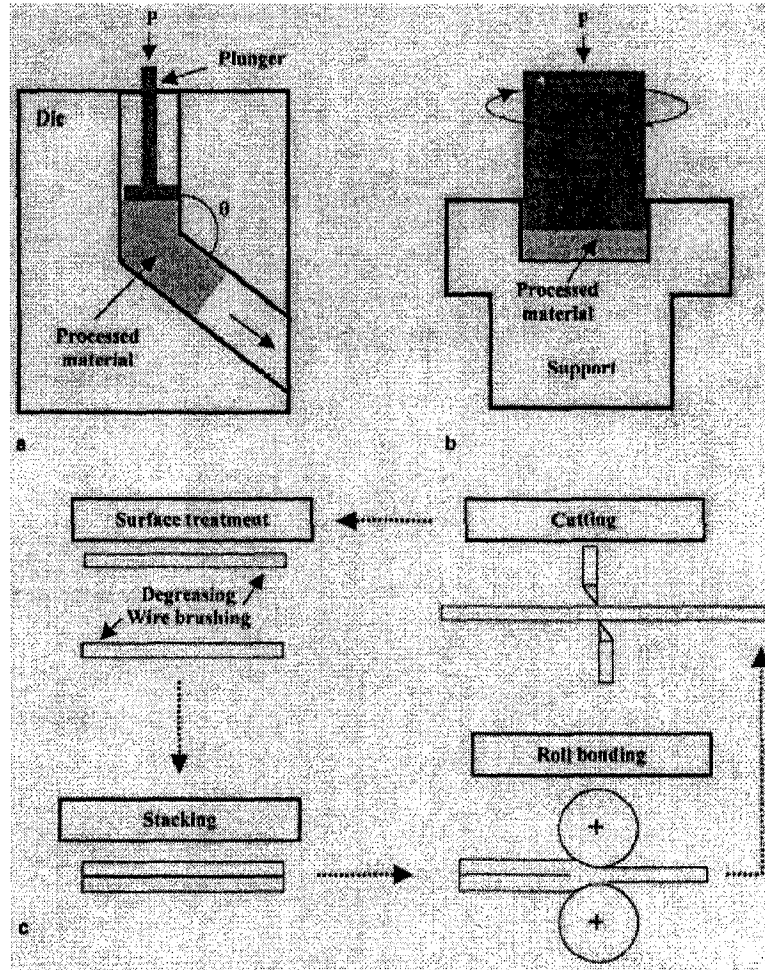


Figure 3.2. Schematic of severe plastic deformation process with (a) equal-channel-angular pressing [3.19], (b) high-pressure torsion [3.19], and (c) accumulative roll-bonding [3.24].

3.1.3. Mechanical Milling

Mechanical milling produces nanostructured materials by the structural disintegration of coarse-grained structures resulting from of severe plastic

deformation [3.25-3.28]. Mechanical milling consists of repeated deformation (welding, fracturing and rewelding) of powder particles in a ball mill until the desired composition is achieved [1.11]. In this process either elemental powder and/or reactive compounds are violently mixed and milled under a protective atmosphere, thereby resulting in chemical homogenization, structural refinement, and even chemical reactions occurring in-situ during milling [3.29, 3.30]. Figure 3.3 shows the set-up for ball milling process.

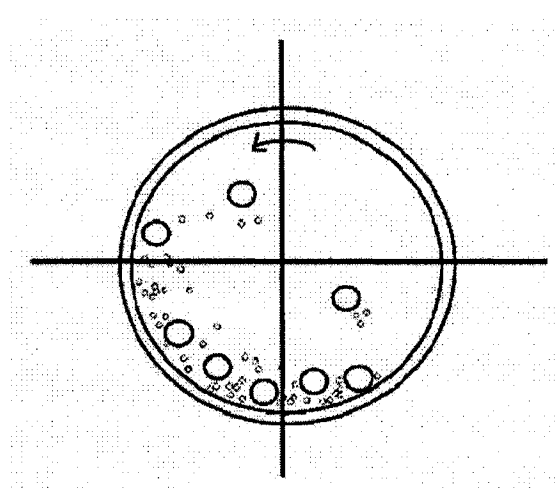


Figure 3.3. Mechanical milling as a means of synthesis of nanostructured material [3.31].

The main processing parameters used to control grain sizes during mechanical milling are continuous or discontinuous milling, the additives, the ball-to-powder weight ratio, ball sizes, milling speed, temperature, and time [3.32-3.34]. The main advantage of mechanical milling is that nanometer-sized grains can be obtained in almost any material after sufficient milling time. However, there are three major shortcomings of this method. These weaknesses include the contamination of the products by either the milling media or the mill atmosphere, possible non-uniform formation of the products within the powder charge of the

mill and partial transformation of the reactants to the products unless a prolonged milling time is used [3.9].

3.1.4. Crystallization of Amorphous Solids

The basic concept behind the crystallization of amorphous solids is the ability to control the crystallization kinetics by optimizing the heat treatment conditions so that the amorphous phase crystallizes completely into a polycrystalline material with ultrafine crystallites [3.35]. Amorphous solids are thermodynamically metastable and will transform into more stable states under appropriate conditions. The driving force for the crystallization is the Gibbs free-energy difference between the amorphous and the crystalline states [3.9]. The amorphous solids can be prepared by a variety of processing routes, such as melt-spinning, splat-quenching, mechanical alloying, vapor deposition, or electrodeposition [3.36]. Crystallization of amorphous solids can be induced by heat treatment [3.37], irradiation [3.38], or mechanical attrition [3.39]. The size of crystallites is strongly dependent on the chemical composition of the amorphous phase and annealing conditions [3.9].

The crystallization of amorphous solids method is easy to control during processing. A wide range of grain sizes can be obtained in the as-crystallized nanocrystalline specimens by simply modifying the heat treatment conditions [3.40]. The main advantage of this method is that it is an efficient way to produce

porosity-free nanocrystalline materials [3.35]. Furthermore, controlled crystallization can be used to obtain partially-crystallized materials with nano-sized precipitates in an amorphous matrix [3.9].

3.1.5. Shock Consolidation

In many applications, nanostructured materials cannot be used in powder form. Thus, powder consolidation is required. The powder consolidation techniques that have been investigated for the consolidation of nanostructured materials are: conventional pressureless sintering [3.41], hot isostatic pressing [3.42], high-pressure/low temperature sintering [3.43, 3.44], plasma activated sintering [3.45, 3.46], and the shock consolidation process [3.47-3.50].

Herring's scaling laws predicted that nanosized particles can be sintered at temperatures several hundred degrees lower than their coarse-grained counterparts because of the short diffusion distance from the contact area to the neck zone of the particles [3.51]. This has been demonstrated in many systems such as nanosized Si_3N_4 , TiO_2 , and TiAl [3.52-3.54]. However, compaction of nanoparticles is known to be difficult because of large specific surface areas and strong friction forces between the particles [3.52]. Typically, pressures as high as several GPa are needed during powder compaction to obtain high green densities [3.43, 3.44].

Most nanomaterials are currently consolidated with non-traditional methods. In the plasma activated sintering process, powders are placed in a graphite die, which is subsequently subjected to on/off electrical discharge pulses for about one minute, which causes sintering [3.45, 3.46]. In the high-pressure/low temperature sintering process, pressures generated via mechanical pressing are often used from 1 GPa to 5 GPa [3.43, 3.44].

Consolidation of powders using high-pressure shock waves is a potentially important method for the synthesis and processing of bulk nanomaterials. This method has been studied since the 1960's and intensively investigated since the 1980's [3.55]. Shock consolidation commonly uses explosives or the impact of high speed projectiles to initiate a shockwave that travels through a confined porous bed of powder. The resulting densification occurs at an extremely high strain rate (10^7 - 10^8 s⁻¹) due to pressure levels exceeding 1 GPa imposed in less than a few microseconds [3.47, 3.48, 3.50, 3.56-3.59]. The extremely short processing time is advantageous for the consolidation of nano-particles since no significant heating of the powder bed occurs, allowing fabrication of bulk samples without the loss of their inherent special characteristics, i.e. no recrystallisation or grain growth [3.56, 3.60].

The advantage of shockwave compaction over conventional routes is the absence of a pressure gradient during compaction, which are common in any regular pressing method. One can expect the possibility of fabricating larger-

scale nanomaterials using dynamic consolidation. The rate at which the pressure is applied on the powder bed might also have an effect on the coalescence of the nanoparticles [3.41-3.46, 3.61-3.63].

Microstructures of materials can be significantly modified and chemical reactivity can be substantially enhanced during shock consolidation. The reaction process can be controlled by altering the starting material characteristics and processing conditions to obtain the desired amount of energy released [3.50]. Figure 3.4 presents an illustration of some of the unique characteristics or effects that occur during shock consolidation of powders [3.50].

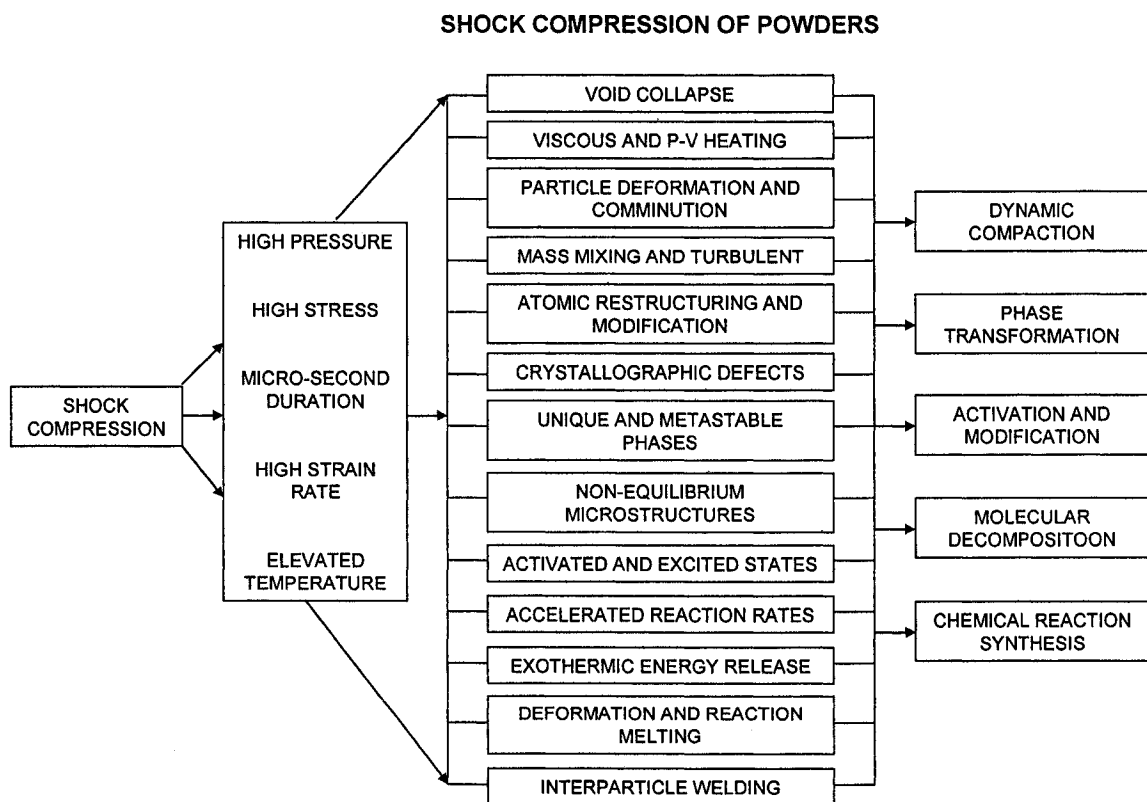


Figure 3.4. Schematic illustrating various processes and their associated effects occurring during shock consolidation of powders [3.50].

Many studies have been performed to estimate the total energy needed to consolidate a powder bed and to determine the shock parameters required to alter consolidation. Meyers et al. [3.48] identified and performed a quantitative evaluation of the various phenomena that occur during the propagation of a shock wave through a powder. They deem this a necessary step to estimate the overall energy requirements for this process. Figure 3.5 presents a schematic representation of these phenomena. The total shock energy is dissipated by the following mechanisms: (1) plastic deformation, (2) microkinetic, (3) melting at interparticle regions, (4) defect formation, (5) friction, (6) fracture, (7) gas compression, and (8) shock initiated chemical reactions.

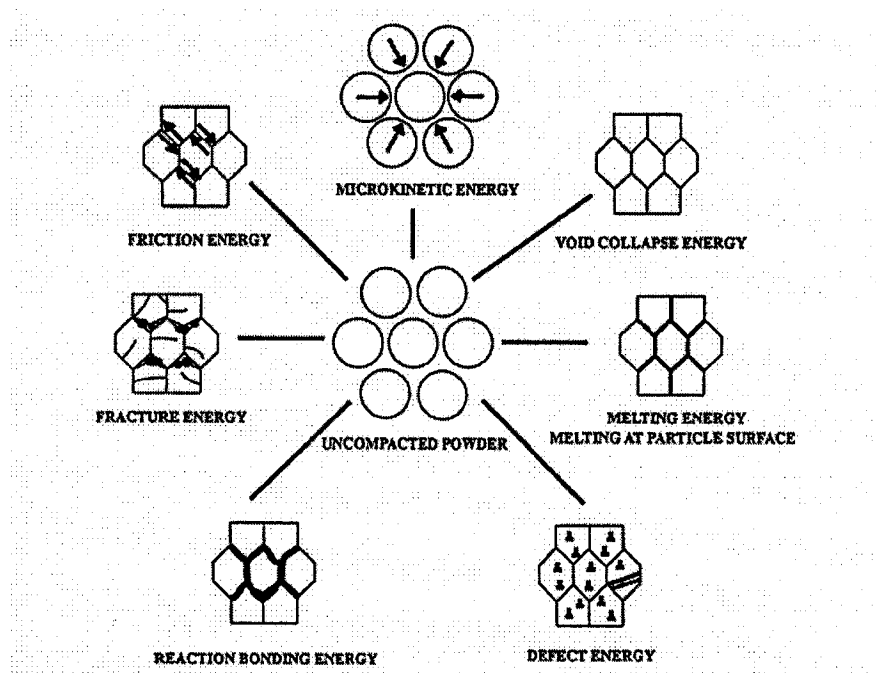


Figure 3.5. Various modes of energy dissipation in shock compression of powders [3.48].

Meyers et al. [3.48] analyzed the shockwave transferred energy which is associated with the void collapse, microkinetic energy and frictional energy that

leads to melting at the powder surfaces, defects (point, line, and interfacial), fractured particles (for brittle materials) and energy release. They indicated that while the energy for shock consolidating a material increases with its strength, all other factors remain constant. It has been observed that larger particles tend to fracture whereas small particles preferentially undergo plastic deformation. It can be seen that the most important energy dissipation processes are: void collapse energy, microkinetic energy, and frictional energy.

Cracking of the compacts at both the microscopic and macroscopic levels due to tensile reflected stresses and residual stresses is a very significant problem in shock consolidation. Meyers and Wang [3.47] described the most common types of cracks as including: (1) circumferential cracks, (2) radial cracks, (3) transverse cracks, (4) mach stem formation, and (5) helicoidal cracks. Figure 3.6 shows the most common types of cracks observed in shock consolidated materials.

As the shock wave propagates through the powders, it generates tensile stresses. These tensile stresses, at the particle level, are accommodated by plastic deformation in ductile materials; cracks are generated within the particles by the activation of existing flaws in brittle materials [3.48]. Kondo and co-workers [3.64-3.66] have successfully implemented an approach in which the reduction of particle size (e.g. nanocrystalline) is used to reduce the flaw size, thereby enabling the application of higher tensile stresses without opening cracks. In addition, Meyers et al. [3.48] recommended a few techniques to

improve shock consolidation including: reduction of tensile stresses by optimized design geometry systems; reduction of shock energy in an effort to improve compact quality; post-shock heat treatments to heal existing flaws and improve the performance of shock compacted powders; and shock densification followed by diffusion bonding.

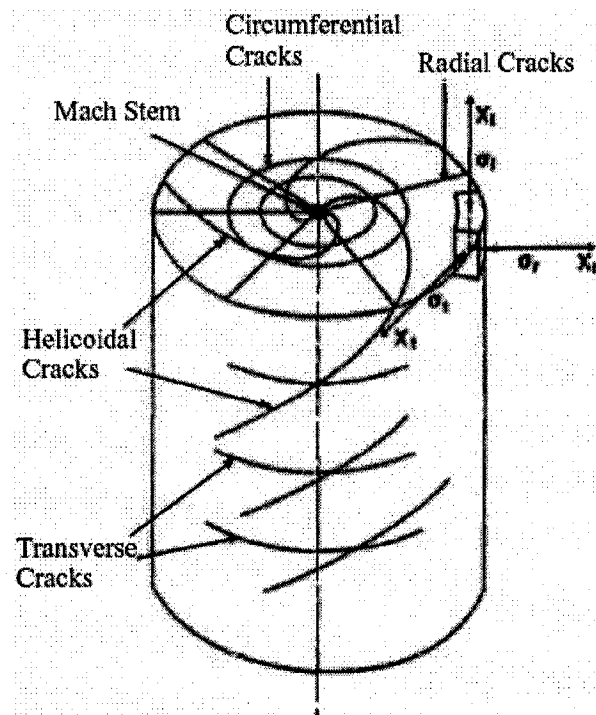


Figure 3.6. Cracks and flaws encountered in shock consolidated cylinders [3.47].

There are several forms of shockwave consolidation processes. The principal methods that have gained acceptance are: explosive shockwave consolidation [3.61, 3.62], dynamic magnetic consolidation [3.63], and gun impact consolidation. Figure 3.7 shows pictures of the three shockwave consolidation processes. In the explosive consolidation process, the powder compact is subjected to very high, shock-generated pressures and deforms adiabatically

locally at particle interfaces in a very short time ($< 1 \mu\text{s}$) [3.61, 3.62]. In the dynamic magnetic compaction process, powder is placed into a conductive tube and then pressed by magnetic force [3.63]. The high currents are pulsed in the coil to produce magnetic fields in the bore. The magnetic fields generated induce current in the armature, which interacts with the magnetic fields to produce an inwardly magnetic force on the tube, consolidating the powder. Pressure up to 2.2 GPa, in a μsec range are obtained. The forces can be applied with great precision. In gun impact compaction, the gun is used to accelerate a flat nose projectile that will impact the specimen.

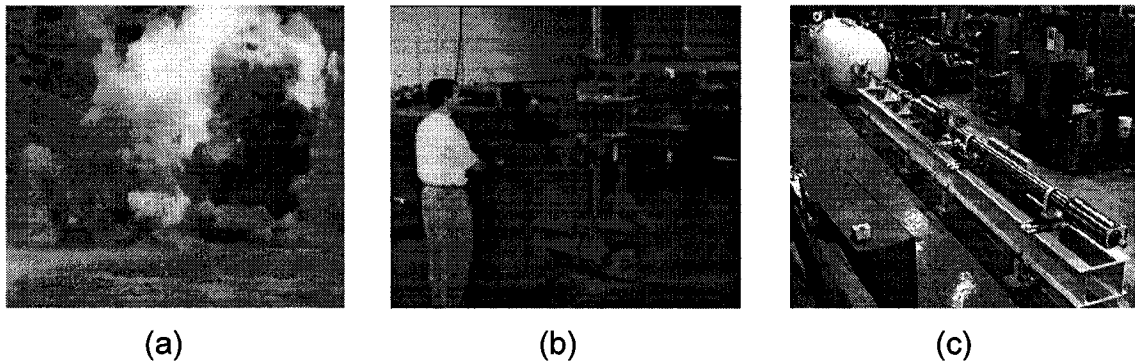


Figure 3.7. Pictures of shockwave consolidation: (a) explosive shockwave consolidation, (b) dynamic magnetic consolidation, and (c) gun impact consolidation

Several experimental fixtures are provided for explosive shockwave consolidation. The CETR/Sawaoka twelve-capsule plate-impact shock recovery system [3.67, 3.68] utilizes an explosively accelerated flyer plate to impact the powders contained in stainless steel capsules. A schematic of the fixture configuration and explosive loading assembly is shown in Figure 3.8 (a). Figure

3.8 (b) shows the cylindrical modified double tube system used by Szewczak et al. [3.69]. After mechanical alloying the powders were cold compacted in cylindrical copper containers and closed with copper plugs.

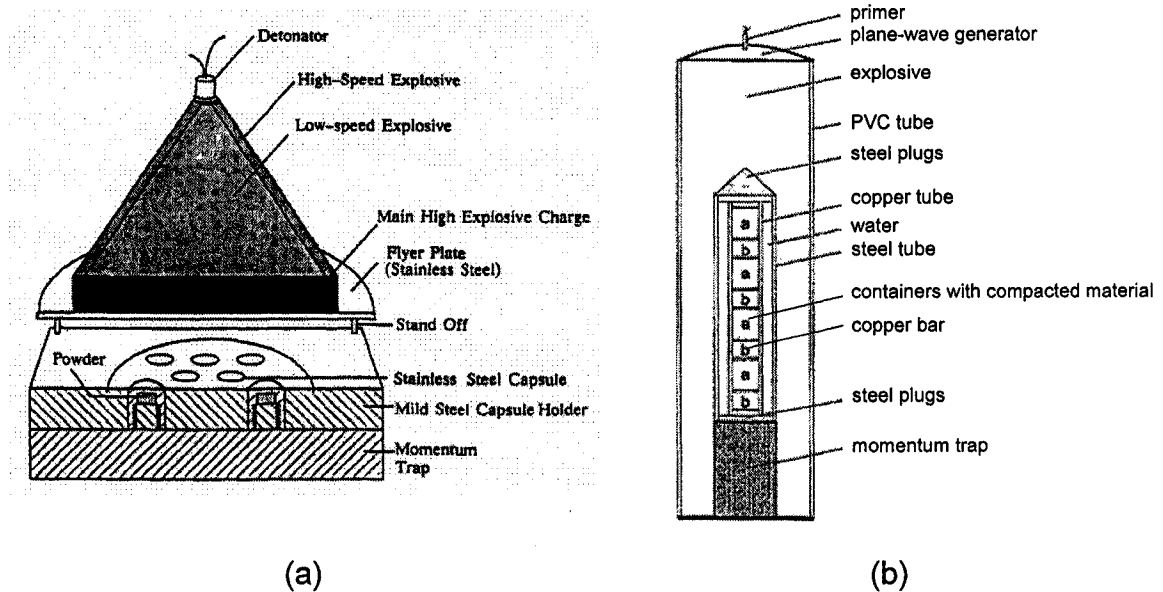


Figure 3.8. (a) Schematic of the CETR/Sawaoka 12-capsule shock recovery fixture configuration and explosive loading system [3.67, 3.68], (b) Cylindrical modified double tube system [3.69].

A typical single-tube experimental fixture is shown in Figure 3.9 (a). The explosion was initiated at the top and the detonation wave propagated downwards, generating high pressures in the capsules, which impacted the metal container. Figure 3.9 (b) shows a symmetrical explosive configuration at longitudinal sections, and a symmetrical loading configuration at cross-sections is shown in Figure 3.9 (c).

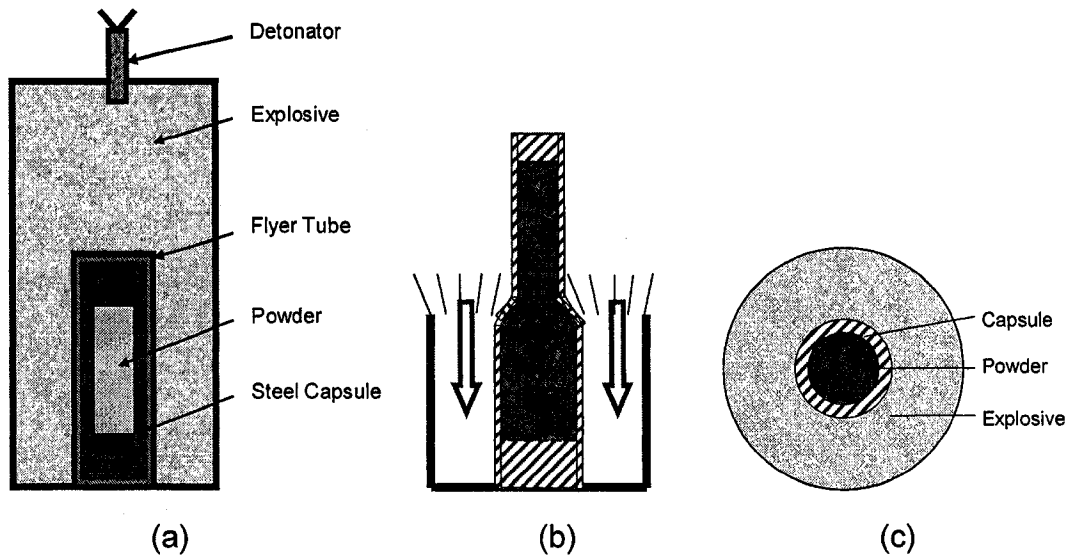


Figure 3.9. (a) Experimental setup, (b) symmetrical explosive configuration (longitudinal sections), and (c) symmetrical loading configuration (cross-sections)

3.2. Properties of Bulk Nanomaterials

Metallic materials may be strong or ductile, but rarely both at once. Strength and ductility are the central mechanical properties of structural materials. The strength and ductility relationship is governed by the physical nature of plastic deformation and artifacts. Nanocrystalline materials exhibit increased strength/hardness [3.70-3.72], reduced toughness, reduced elastic modulus and ductility, enhanced diffusivity [3.73], higher specific heat, an enhanced thermal expansion coefficient, and superior soft magnetic properties in comparison with conventional polycrystalline materials [1.11].

The following sections present a brief description of the previously listed properties.

3.2.1. Elastic Properties

Early measurements of the Young's modulus, E , on nanocrystalline materials prepared by the inert gas condensation method gave lower values than the previously measured values for conventional grain size materials [3.74]. Figure 3.10 shows the Young's modulus as a function of porosity for nanocrystalline Pd and Cu as shown by Weertman et al. [1.12]. Krstic et al. [3.75] have suggested that the presence of extrinsic defects (pores and cracks) was responsible for the reduction of Young's modulus. Subsequent work on porosity-free materials has supported these conclusions.

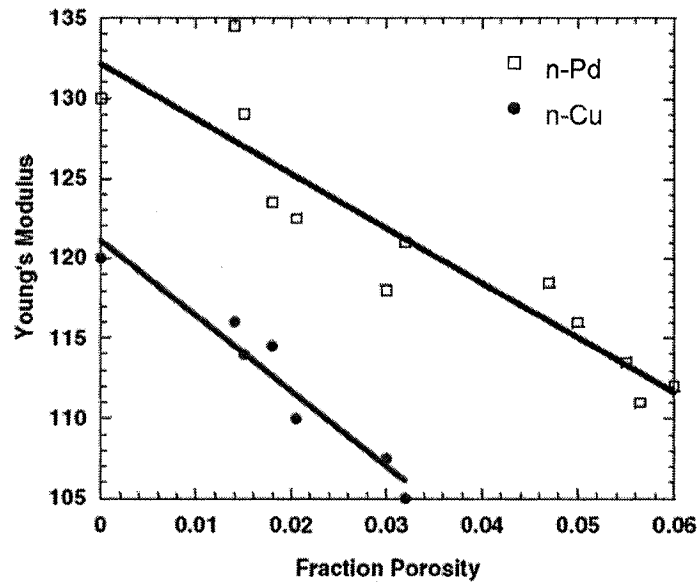


Figure 3.10. *Young's modulus as a function of porosity for nanocrystalline Pd and Cu [1.12].*

Wachtman and MacKenzie [3.76, 3.77] expressed the relationship between Young's modulus E , and porosity p , in Eq. 3.1:

$$E = E_0(1 - 1.9p + 0.9p^2) \quad (\text{Eq. 3.1})$$

For relatively low porosity materials, p^2 can be neglected. The yield stress and tensile ductility are simultaneously affected [1.11].

It is now believed that the intrinsic elastic modulus of nanostructured materials are essentially the same as those for conventional grain size materials until the grain size becomes < 20 nm, when the number of atoms associated with the grain boundaries and triple junctions becomes very large [3.74]. As described in Figure 3.11, Shen et al. [3.78] have demonstrated the relationship between Young's modulus and grain size using nanocrystalline Fe prepared by mechanical attrition and measured by a nano-indentation technique.

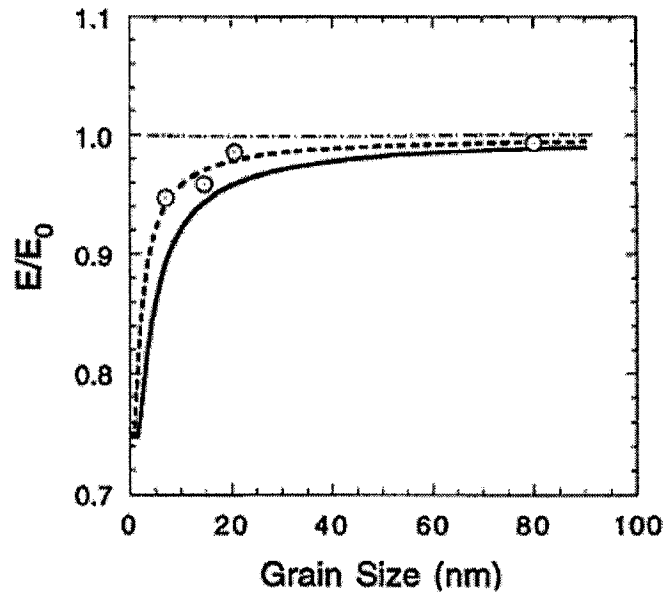


Figure 3.11. Ratio of the Young's modulus of nanocrystalline materials to those of conventional grain size materials as a function of grain size [3.78].

The dashed and solid lines correspond to a grain boundary thickness of 0.5 and 1 nm, respectively. The open circles show the E/E_0 values. The horizontal dotted-dashed line represents the E/E_0 ratio for materials having an infinite grain size [3.78]. Thus, for most nanostructured materials for which grain size > 10 nm, the elastic modulus does not possess unique properties [3.74].

3.2.2. Hardness and Strength

Grain size has a significant effect on the mechanical behaviour of materials, especially hardness and strength. For ductile polycrystalline materials, the Hall - Petch equation has been found to express the grain-size dependence of flow stress on grain size, as shown by equation 3.2 [1.11].

$$\sigma_y = \sigma_0 + kd^{-1/2} \quad (\text{Eq. 3.2})$$

In the above equation, σ_y is yield stress, d is grain diameter, σ_0 is a materials constant for the starting stress for dislocation movement, and k is a material constant for the fitting parameter. This is indeed an approximation, and a more general formulation can be achieved by using a power expression with exponent $-n$, where $0.3 \leq n \leq 0.7$ [1.11]. To explain the empirical observations, several models have been proposed, which involve either dislocation pileups at grain boundaries or grain boundary dislocation networks as dislocation sources. In all cases the Hall - Petch effect is due to dislocation motion/generation in materials that exhibit plastic deformation [3.74].

The relation of yield stress on grain size in metals is well established in micrometer and larger sized grains. The yield strength of nanocrystalline materials has been measured and there is a consensus that the Hall - Petch relationship breaks down with a decrease in slope in the 1 μm – 100 nm range. However, experimental results on materials show there is ambiguity in the trend of the plot for grain sizes of 100 nm or lower ($d^{-1/2} > 0.1 \text{ nm}^{-1/2}$). Some results show a decrease in the yield stress (negative Hall – Petch slope), some show an increase (positive Hall – Petch slope), and others show a plateau [1.11]. The scatter reports can be seen in Figure 3.12, which shows the Hall - Petch plot for Cu taken from different sources [1.11]. Most data [3.79-3.82] exhibit the negative Hall - Petch effect at small grain sizes. It is suggested that the procedure used to study the grain size dependence may result in changes in the structure such as densification, stress relief, phase transformations, or grain boundary structure, all of which may be artifacts and could explain the observed negative Hall - Petch behavior [3.79].

For all strain rates, the stress first increased and then decreased as the grain size was reduced. The total strain rate of the crystallite was calculated by considering contributions from the dislocation, the boundary diffusion and the lattice diffusion mechanisms [1.11]. The dominant deformation mechanisms for the crystallite phase as a function of grain size are depicted in Figure 3.13. The deformation mechanisms of the grain-boundary phase were modeled as a diffusional flow of matter through the grain boundary.

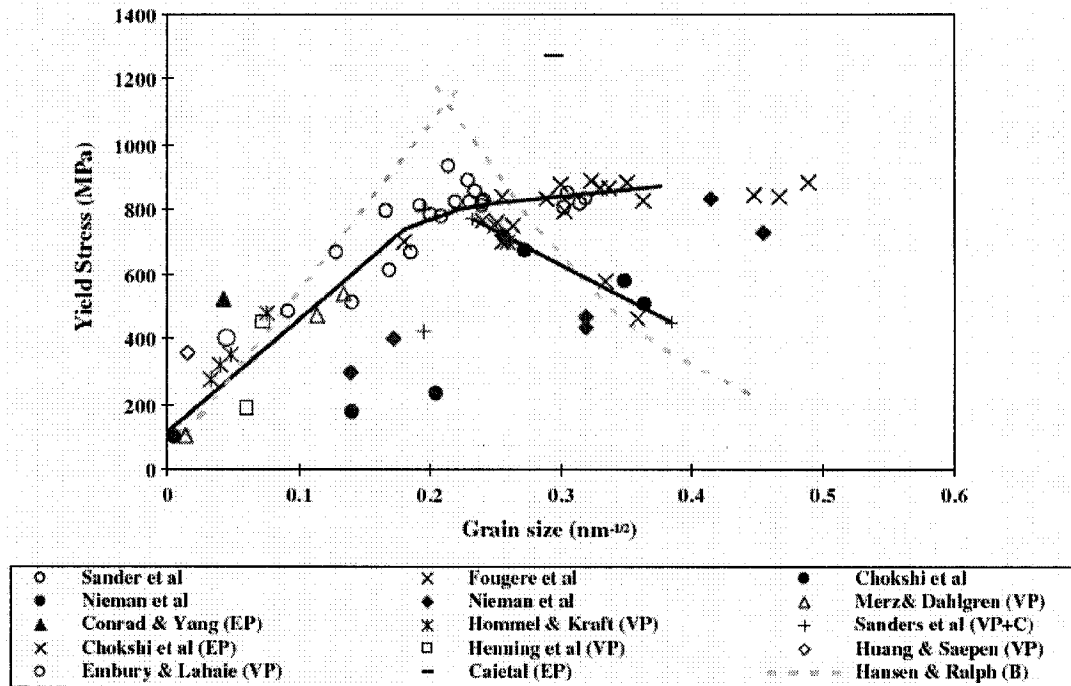


Figure 3.12. Compiled yield stress versus grain size plot for Cu from various sources ranging from coarse to nanograin size. The plots show different trends as the grain size falls below a critical size [1.11].

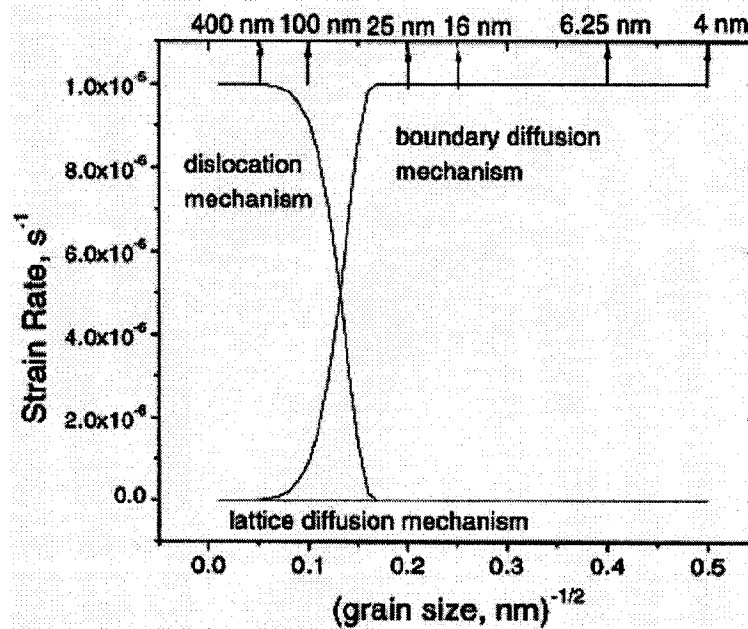


Figure 3.13. Grain size dependence of all three contributions to the total imposed strain (dislocation mechanism, grain-boundary diffusion and lattice diffusion mechanism) in Cu for the total imposed strain rates of 10^{-3} s^{-1} [3.83].

Meyers et al. [3.84] have summarized the major mechanisms for the four grain domains. In the region of $1\ \mu\text{m} - 100\ \text{nm}$, the described models are based on dislocation generation at or adjacent to grain boundaries and on the formation of work-hardened grain boundary layers. In the range of $100\ \text{nm} - 20\ \text{nm}$, the dislocations emitted from grain boundaries have an increasingly reduced probability of cross-slipping and multiplying in grains, which leads to shear localization. In the regime of $20\ \text{nm} - 1\ \text{nm}$, the grain boundary effects dominate the deformation process. In the regime of $1\ \text{nm} - 0\ \text{nm}$, deformation is dominated by regions of intense shear [3.84].

Most of the mechanical property data on nanocrystalline materials have pertained to hardness. The experimental results of hardness measurements can be summarized as follows. In general, grain size is reduced through the nanoscale regime ($< 100\ \text{nm}$), hardness typically increases with decreasing grain size and can be factors of 2 to 7 times harder for pure nanocrystalline metals (10 nm grain size) than for large-grained ($> 1\ \mu\text{m}$) metals [3.79-3.82].

3.2.3. Ductility and Toughness

It is known that grain size has a strong effect on the ductility and toughness of conventional grain size ($> 1\ \mu\text{m}$) materials, usually a reduction in grain size leads to an increase in ductility and toughness. Koch et al. [3.85] have reported that materials processing elongation of 40–60% in the conventional grain size range is reduced to nearly nil when grain size is smaller than 25 nm. Unfortunately, the

low ductility of nanomaterials is an artifact caused by the presence of defect. Figure 3.14 illustrates the elongation to failure rate in tension vs. grain size for some nanocrystalline metals and alloys [3.74]. It has been observed that pure nanocrystalline metals exhibit essentially brittle behaviour for grain sizes < 30 nm, while displaying significant ductility for conventional grain sizes. The results of ductility measurements on nanocrystalline metals [3.86-3.93] are contradictory and directly related to flaws and porosity, surface finish, and method of testing (e.g., tension or compression testing). Also, deformation mechanisms significantly affect the ductility of nanocrystalline metals.

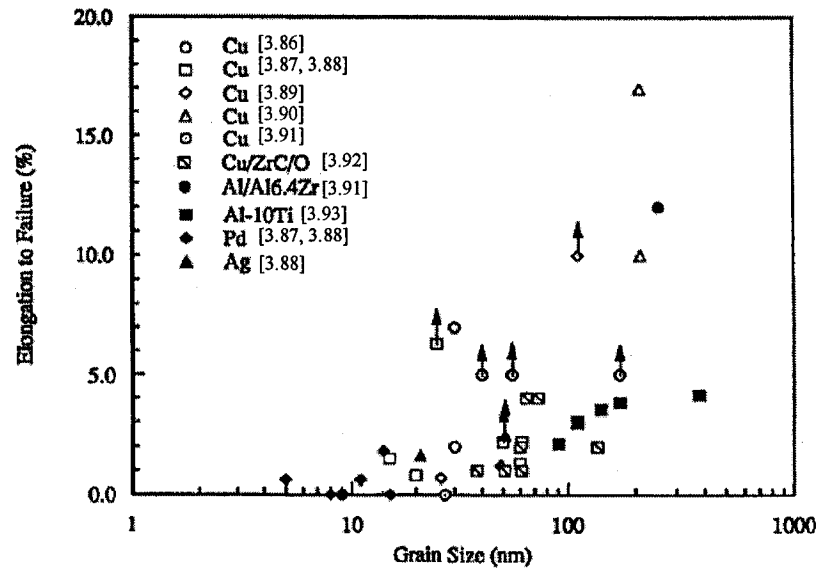


Figure 3.14. Elongation to failure in tension vs. grain size for some nanocrystalline metals and alloys [3.74].

Figure 3.15 shows data on normalized yield strength (strength/strength of conventional polycrystalline) versus percentage elongation in tension for metals. Figure 3.15(a) exhibits a clear decrease in ductility as strength is increased with grain sizes in the nanocrystalline range. In comparison, Figure 3.15(b) exhibits

the increased yield strength along with good ductility in the ultrafine grained materials (100–500 nm) range [3.94].

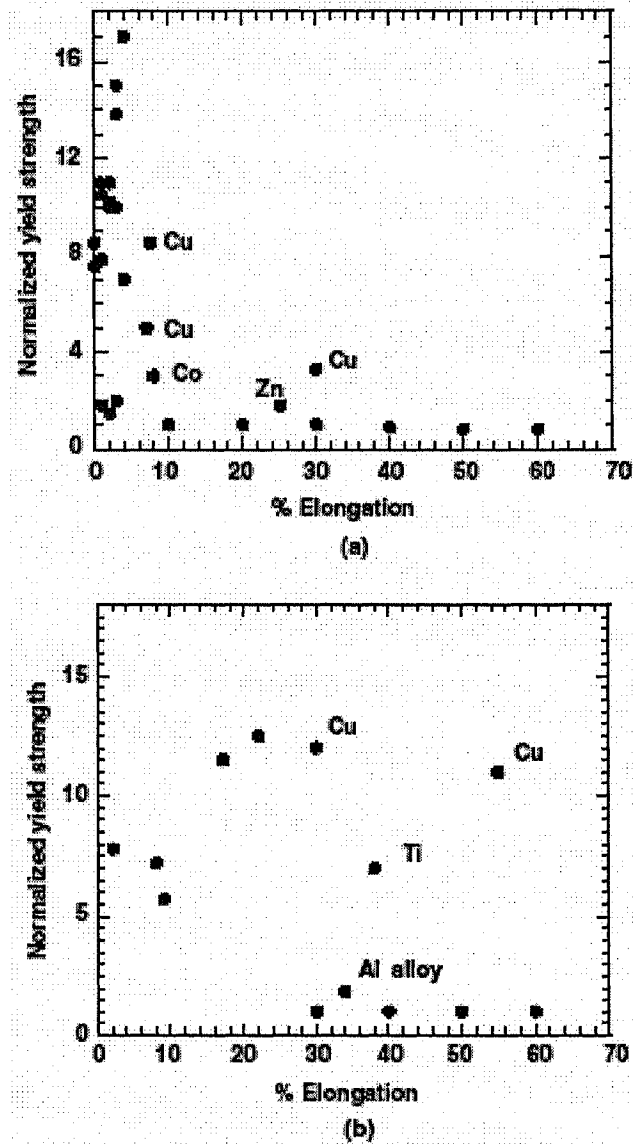


Figure 3.15. Compilation of yield stress versus % elongation of (a) nanocrystalline metals, (b) ultrafine grained metals [3.94].

Unfortunately, it is difficult to process nanostructured materials free from the artifacts that mask their inherent mechanical properties. Ma [3.95] reviewed

various routes to improve the tensile ductility of bulk nanostructured metals and alloys. The methods identified by Ma are as follows : (1) creating a bimodal grain size distribution [3.96-3.98]; (2) a mixture of two or multiple phases with varying size scales and properties [3.99, 3.100]; (3) using nanoscale growth twins in lieu of the nanograins for strengthening [3.101, 3.102]; (4) dispersions of nanoparticles and nano-precipitates [3.94]; (5) using transformation-induced plasticity [3.103]; (6) lowering of dynamic recovery at low-temperature and/or dynamic strain rates [3.104-3.106]; (7) improving strain rate hardening [3.105]; and (8) fabrication of flawless materials [3.107-3.109].

In consolidated nanostructured materials, porosity reduces strength and helps to initiate shear localization. Therefore, processing truly flaw-free materials is the requirement that is paramount for consolidated nanostructured materials. A breakthrough has been achieved for obtaining a full density consolidated nanostructured Cu [3.107-3.109], which is remarkably strong and ductile. Figure 3.16 shows a typical tensile stress-strain curve for the bulk in situ consolidated nanocrystalline Cu sample, with a relatively narrow lognormal grain size distribution with an average grain size of 23 nm [3.108]. In comparison to Figure 3.16, a coarse-grained polycrystalline Cu sample with an average grain size larger than 80 μm and a curve representative of previous nanocrystalline Cu samples prepared by an inert-gas condensation with a mean grain size of 26 nm [3.110] have also been included for comparison.

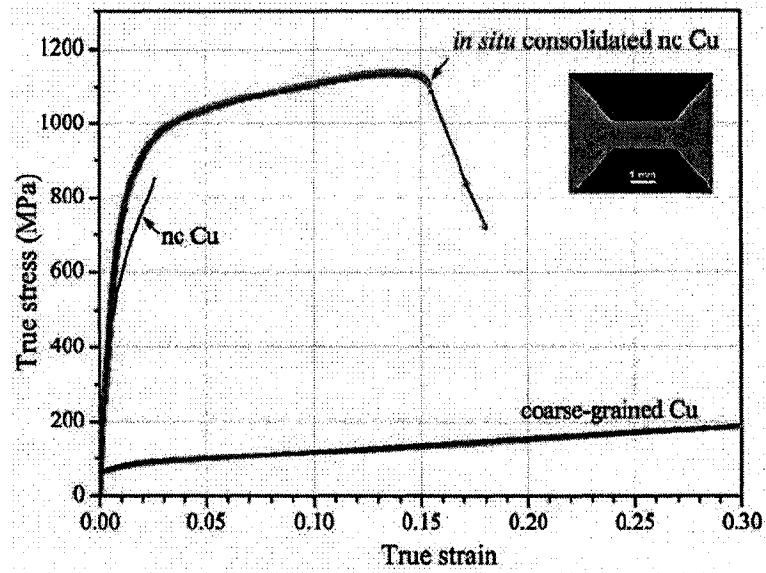


Figure 3.16. A typical tensile stress-strain curve [3.108] for the bulk *in situ* consolidated nanocrystalline Cu sample, in comparison with that of a coarse-grained polycrystalline Cu sample and a nanocrystalline Cu sample prepared by an inert-gas condensation and compaction technique [3.110].

For polycrystalline materials (grain sizes $>1\ \mu\text{m}$) toughness and strength are superior in microstructures with finer grain size [3.111, 3.112]. Grain refinement increases the yield and fracture strength simultaneously and reduces the ductile to brittle transition temperature, thus improving toughness. However, for the nanocrystalline and ultrafine-grained materials, Erb et al. [3.113] have reported that they did not observe the positive effects of grain size reduction on impact toughness for the Co materials with grain sizes between 18 nm to 10 μm . Their work shows that the modulus of toughness values derived from thin tensile specimens tested under quasi-static conditions are not comparable with toughness values obtained from impact testing on thicker material [3.113-3.115].

3.3. References

- [3.1] Gleiter H., Materials with ultrafine grain size. In: Hansen N, editor. Deformation of polycrystals: mechanisms and microstructures. Roskilde: Risø National Laboratory 1981; p. 15.
- [3.2] Nieh T.G., Luo P., Nellis W., Lesuer D., Benson D., Acta mater 1996;44:3781
- [3.3] Verhoeven J., Fundamentals of Physical Metallurgy. New York (NY): John Wiley & Sons, 1975. p. 204.
- [3.4] Lee J., Zhou F., Chung K.H., Kim N.J., Lavernia E.J., Metallurgical and Materials Transactions A 2001;32:3109
- [3.5] Lowenheim F.A., Electroplating, New York: McGraw-Hill Book Co., 1978.
- [3.6] Erb U., Nanostruct Mater 1995;6:533–8.
- [3.7] Cheungetal C., Nanostruct. Mater., 5(5) (1995), p. 513-523.
- [3.8] Wang N. et al., Mater. Sci. Eng., A237 (1997), p. 150-158.
- [3.9] Shaw L.L., JOM; Dec 2000; 52, 12; p. 41
- [3.10] Iwahashi Y., Wang J.T., Horita Z., Nemoto M., Langdon T.G., Scripta Mater 1996; 35:143–6.
- [3.11] Iwahashi Y., Horita Z., Nemoto M., Langdon T.G., Acta Mater 1998;46:3317–31.
- [3.12] Nemoto M., Horita Z., Furukawa M., Langdon T.G., Met Mater Intl 1998;4:1181–90.
- [3.13] Langdon T.G., Furukawa M., Nemoto M., Horita Z., J Miner Metals Mater Soc 2000;52:30–3.
- [3.14] Furukawa M., Horita Z., Nemoto M., Langdon T.G., J Mater Sci 2001; 36:2835–43.

- [3.15] Horita Z., Fujinami T., Langdon T.G., Mater Sci Eng A—Struct Mater Properties Microstruct Process 2001;318:34–41.
- [3.16] Horita Z., Lee S., Ota S., Neishi K., Langdon T.G., Superplast Adv Mater, Icsam-2000 2001;357:471–6.
- [3.17] Furukawa M., Horita Z., Nemoto M., Valiev R.Z., Langdon T.G., Mater Characteriz 1996;37:277–83.
- [3.18] Popov A.A. et al., Scr. Mater., 37(7) (1997), p. 1089-1094.
- [3.19] Valiev R.Z., Mater. Sci.Eng., A234-236 (1997), p. 59-66.
- [3.20] Ferrasse S. et al., Metal. Mater. Trans., 28A (1997), p. 1047.
- [3.21] Kawazoe M. et al., Scr. Mater., 36(6) (1997), p. 699-705.
- [3.22] Valiev R.Z. et al., Acta Metall. Mater., 42(1994), p. 2467.
- [3.23] Tsuji N. et al., Scr. Mater., 40(7) (1999), p. 795-800.
- [3.24] Saito Y. et al., Scr. Mater., 39(9) (1998), p. 1221-1227.
- [3.25] Suryanarayana C., Prog Mater Sci 2001;46:1–184.
- [3.26] Fecht H.J., Hellstern E., Fu Z., Johnson W.L., Metall Trans A 1990;21:2333.
- [3.27] Eckert J., Holzer J.C., Krill III C.E., Johnson W.L., J Mater Res 1992;7:1751.
- [3.28] Fecht H.J., Nanophase materials. In: Hadjipanayis GC, Siegel RW, editors. vol. 260; 1994. p. 125.
- [3.29] Schaffer G.B., McCormick P.G., Metall. Trans., 21A (1990), p. 2789-2794.
- [3.30] Davis R.M., McDermott B., Koch C.C., Metall. Trans., 19A (1988), p. 2867-2874.

- [3.31] Zhou F., Liao X.Z., Zhu Y.T., Dallek S., Lavernia E.J., *Acta Mater* 2003;51:2777–91.
- [3.32] Schaffer G.B., McCormick P.G., *Metall. Trans.*, 22A (1991), p. 3019-3024.
- [3.33] Schaffer G.B., McCormick P.G., *Metall. Trans.*, 23A (1992), p. 1285-1290.
- [3.34] Yang Z.G., Shaw L., *Nanostruct. Mater.*, 7(8) (1996), p. 873-886.
- [3.35] Lu K., *Mater. Sci. Eng.*, 1996;R16(4):161–221.
- [3.36] Liebermann H.H., *Amorphous metallic alloys*. In: Luborsky, FE, editor; 1988. p. 26.
- [3.37] Scott M.G., *Amorphous Metallic Alloys*. In: Luborsky FE; 1988. p. 144.
- [3.38] Azam N., Lenaour L., Rivera S., Grosjean P., Sacovy P., Delaplace J., *J Nucl Mater* 1979;83:298.
- [3.39] Luborsky F.E. et al., *Amorphous Metallic Alloys*, London: Butterworth, 1983.
- [3.40] Lu K., Wang J.T., Wei W.D., *J. Appl. Phys.*, 69(1) (1991), p. 522-524.
- [3.41] Ungar T. et al., *Nanostruct. Mater.*, 11(1) (1999), p. 103-113.
- [3.42] Hojo J. et al., *Key Engineering Materials*, 161-163 (1999), p. 465-468.
- [3.43] Liao S.C., Mayo W.E., Pae K.D., *Acta Mater.*, 45(10) (1997), p. 4027-4040.
- [3.44] Gutmanas E.Y., Rabinkin A., *Scripta Metal.*, 13(1979), p. 11-15.
- [3.45] Risbud S.H., Shan C.H., *Mater. Sci. Eng.*, A204 (1995), p. 146-151.
- [3.46] Yoo S.H. et al., *Nanostruct. Mater.*, 12(1-4) (1999), p. 23-28.

- [3.47] Meyers M.A., Wang S.L., *Acto metall.* Vol. 36, No. 4, p. 925-936, 1988.
- [3.48] Meyers M.A., Benson D.J., Olevsky E.A., *Acta Mater.* Vol. 47, No. 7, p. 2089-2108, 1999.
- [3.49] Meyers M.A., Batsanov S.S., Gavrilkin S.M., Chen H.C., LaSalvia J.C., Marquis F.D.S., *Materials Science and Engineering A201* (1995), p. 150-158.
- [3.50] Thadhani N.N., *Progress in Materials Science* 1993, Vol. 37, p. 117-226.
- [3.51] Herring C., *J. Appl. Phys.*, 21(1950), p. 301-303.
- [3.52] Pechenik A., Piermarini G.J., Danforth S.C., *J. Am. Ceram. Soc.*, 75(12) (1992), p. 3283-3288.
- [3.53] Hofler H.J., Averback R.S., *Scripta Metall. Mater.*, 24(1990), p. 2401-2406.
- [3.54] Froes F.H. et al., *JOM*, 44(5) (1992), p. 26-28.
- [3.55] Prummer R., *Explosivverdichtung Pulveriger Substanzen*. Springer, Berlin, 1987.
- [3.56] Korth G.E., Williamson R.L., *Metallurgical and Materials Transactions - Series A* 1995;26:2571
- [3.57] Nesternko V.F., *Cornbust. Explos. Shock Waves* 1986;21:730
- [3.58] Gourdin W.F., *J. appl. Phys.* 1984;55:172
- [3.59] Sivakumar K., Raj P.S., Bhat T.B., Hokamoto K., *J. Mater. Process. Technol.* 2001;115:396
- [3.60] Stueadhammer K.P., Johnson K.A., Controlled powder morphology experiments in megabar 304L stainless steel compaction. In: Murr LE, Stueadhammer KP, Meyers MA, editors. *Metallurgical Application of Shock-wave and High-strain-rate phenomena*, Marcel Dekker (NY): 1986. p. 149.
- [3.61] Morris D.G., *Mater. Sci. Eng.*, 57(1983), p. 187.

- [3.62] Cline C.F., Hopper R.W., *Scr. Metall.*, 11(1977), p. 1137.
- [3.63] Chelluri B., Barber J.P., *JOM*, 51(7) (1999), p. 36-37.
- [3.64] Kondo, K.I., Soga, S., Sawaoka, A., Araki M., *J. Mater. Sci.*, 1985, 20, p. 1033.
- [3.65] Kondo, K.I., Sawai, S., *J. Am. Ceram. Soc.*, 1990, 73(7), 1983.
- [3.66] Kondo, K.I., Sawai, S., in *Science and Technology of New Diamond*, ed. S. Saito, O. Fukunaga and M. Yoshikawa. K. T. K. Science, Tokyo, 1990, p. 245.
- [3.67] Akashi, T.K., Sawaoka, A.B., U.S. Patent 4,655,830, April 7, 1987.
- [3.68] Thadhani, N.N., *The CETR/Sawaoka 12-Capsule Shock Impact Recovery Fixture: Design and Experimentation*, CETR Report, New Mexico Tech, Socorro, New Mexico, July 1990.
- [3.69] Szewczak E., Paszula J., Leonov A.V., Matyja H., *Materials Science and Engineering A226-228* (1997) p. 115-118
- [3.70] Hall E.O., *Proc Phys Soc B* 1951;64:747.
- [3.71] Petch N.J., *J Iron Steel Inst* 1953;174:25.
- [3.72] Ashby M.F., *Philos Mag A* 1982;46:737.
- [3.73] Wurschum R., Herth S., Brossmann U., *Adv Eng Mater* 2003;5:365–72.
- [3.74] Koch C., *Bulk Behavior of Nanostructured Materials*, North Carolina State University
- [3.75] Krstic, V., Erb U., Palumbo G., 1993. *Scripta Metall. et Mater.* 29:1501.
- [3.76] Wachtman J.B., In: Wachtman JB, editor. *Mechanical and thermal properties of ceramics*. NBS Washington: NBS Special Publication; 1963. p. 139.

- [3.77] MacKenzie J.K., Proc Phys Soc B 1950;63:2.
- [3.78] Shen, T.D., Koch C.C., Tsui T.Y., Pharr G.M., 1995. J. Mater. Res. 10:2892.
- [3.79] Siegel R.W., Fougere G.E., 1994. In Nanophase materials, ed. G.C. Hadjipanayis and R.W. Siegel. Netherlands: Kluwer Acad. Publ., 233-261.
- [3.80] Weertman, J.R., Averback R.S., 1996. In Nanomaterials: Synthesis, properties, and applications, ed. A.S. Edlestein and R.C. Cammarata. Bristol: Institute of Physics Publ., 323-345.
- [3.81] Morris D.G., Morris M.A., 1997. Materials Science Forum 235-238:861.
- [3.82] Siegel. R.W., 1997. Materials Science Forum 235-238:851.
- [3.83] Kim H.S., Estrin Y., Bush M.B., Acta Mater 2000;48:493–504.
- [3.84] Meyers M.A., Mishra A., Benson D.J., JOM, 2006 , v. 58 , n. 4 , p. 41.
- [3.85] Koch C.C., Morris D.G., Lu K., Inoue A., MRS Bull 1999;24:54.
- [3.86] Günther, Baalman B.A., Weiss. H., 1990. Mater. Res. Soc. Symp. Proc. 195:611-615.
- [3.87] Nieman, G.W., Weertman J.R., Siegel. R.W., 1991. Mater. Res. Soc. Symp. Proc. 206:581-586.
- [3.88] Nieman, G.W., Weertman J.R., Siegel. R.W., 1991. J. Mater. Res. 6:1012-1027.
- [3.89] Sanders, P.G., Eastman J.A., Weertman J.R., 1996. In Processing and properties of nanocrystalline materials, ed. Suryanarayana et al. 1996, 379-386
- [3.90] Gertsman, V.Y., Hoffman M., Gleiter H., Birringer R., 1994. Acta Metall. Mater. 42:3539-3544.

- [3.91] Eastman, J.A., Choudry M., Rittner M.N., Youngdahl C.J., Dollar M., Weertman J.R., DiMelfi R.J., Thompson L.J., In Chemistry and physics of nanostructures, ed. Ma et al. 1997, 173-182
- [3.92] Morris D.G., Morris. M.A., 1991. *Acta Metall. Mater.* 39:1763-1779.
- [3.93] Liang, G., Li Z., Wang. E., 1996. *J. Mater. Sci.*
- [3.94] Koch C.C., *Scripta Mater* 2003;49:657–62.
- [3.95] Ma E., *JOM*, 2006 , v. 58 , n. 4 , p. 49.
- [3.96] Zhang X., Wang H., Scattergood R.O., Narayan J., Koch C.C., *Acta Mater* 2002;50:3995.
- [3.97] Zhang X., Wang H., Scattergood R.O., Narayan J., Koch C.C., *Acta Mater* 2002;50:3527.
- [3.98] Zhang X., Wang H., Scattergood R.O., Narayan J., Koch C.C., *Acta Mater* 2002;50:4823.
- [3.99] Dai Q.L. et al., *Mater.Res.*, 19 (2004), p. 2557.
- [3.100] Sun B.B. et al., *Acta Mater.*, 54 (2006), p. 1349.
- [3.101] Lu L. et al., *Science*, 304 (2004), p. 422.
- [3.102] Ma E. et al., *Appl. Phys. Lett.*, 85 (2004), p. 4932.
- [3.103] Wu X. et al., *Scripta mater.*, 52 (2005), p. 547.
- [3.104] Wang Y.M., Ma E., *Acta Mater.*, 52 (2004), p. 1699.
- [3.105] Wang Y.M., Ma E., *Appl. Phys. Lett.*, 83 (2003), p. 3165.
- [3.106] Wang Y.M., Ma E., *Advanced Mater.*, 16 (2004), p. 328.

- [3.107] Cheng S. et al., *Acta Mater.*, 53 (2005), p. 1521.
- [3.108] Youssef K.M., Scattergood R.O., Murty K.L., Horton J.A., Koch C.C., *Appl. Phys. Lett.* Vol. 87, 091904, (2005)
- [3.109] Youssef K.M. et al., *Appl. Phys. Lett.*, 85 (2004), p. 929.
- [3.110] Legros M., Elliott B.R., Rittner M.N., Weertman J.R., Hemker K.J., *Philos. Mag. A* 80, 1017 (2000).
- [3.111] Hertzberg R.W., *Deformation and Fracture Mechanics of Engineering Materials*, second ed., Wiley, New York, 1976, p. 325.
- [3.112] Dieter G.E., *Mechanical Metallurgy*, third ed., McGraw Hill, New York, 1987, p. 471.
- [3.113] Karimpoor A.A., Aust K.T., Erb U., *Scripta Materialia*, V 56, Issue 3, February 2007, p. 201-204
- [3.114] Karimpoor A.A., Erb U., Aust K.T., Palumbo G., *Scripta Mater.* 49 (2003) p. 651.
- [3.115] Karimpoor A.A., Erb U., Aust K.T., Wang Z., Palumbo G., *Mater. Sci. Forum* 386–388 (2002), p. 415.

CHAPTER 4

FABRICATION OF BULK NANOSTRUCTURED SILVER MATERIAL FROM NANOPOWDERS USING SHOCKWAVE CONSOLIDATION TECHNIQUE

4.1. Introduction

One of the major challenges in fabricating large scale nano-structured components is to optimize fabrication processes while maintaining the microstructure at a nanometer scale during consolidation [3.4]. The powder metallurgy route is one of the viable processes that have been identified for fabricating bulk nanostructure materials. With this approach, two sources of raw materials are available, specifically nano-sized and nanostructured powder. Nano-sized powder consists of a single crystal with nano-scale particle size distribution while nanostructured powder is composed of micron-scale particles possessing a nanograin structure. The following discussion will be oriented towards the nano-sized powder. Transport processes responsible for sintering are significantly altered by the nano-scale size since the grain size is similar to

the characteristic length of the transfer process [4.1]. The short diffusion distances within nano-sized powders are beneficial as they enhance the processing kinetics. Nevertheless, the short diffusion distances can also be detrimental since the driving force and rate of grain growth is increased [4.1]. Consequently, the optimization of traditional consolidation processes is essential in order to obtain a fully densified sample and the desired nanostructure [4.2].

Shock consolidation of nano-size powders is an approach that has the potential to process large-scale bulk nanomaterials [4.3]. Shock consolidation commonly uses explosives or the impact of high speed projectiles to initiate a shockwave that travels through a confined porous bed of powder. The resultant densification occurs at an extremely high strain rate (10^7 - 10^8 s⁻¹) due to pressure levels exceeding 1 GPa imposed in less than a few microseconds [3.47, 3.48, 3.50, 3.56-3.59]. The extremely short processing time is advantageous for consolidating nano-particles as no significant heating of the powder bed occurs, allowing fabrication of bulk samples without the loss of their inherent special characteristics, i.e. no recrystallisation or grain growth [3.56, 3.60]. Inspection of the available literature uncovered limited information available on the few systems tested. Nieh et al. [3.2] investigated the shock-compaction behavior of aluminum nanocrystals possessing an average particle size of about 50-70 nm, and where, after shock consolidation, the average grain size ranged between 80-200 nm. Unfortunately, no investigation of the mechanical properties was reported.

The present work focuses on the fabrication and characterization of shock consolidation bulk nanostructured silver components from nano-size powder. The silver system was selected because it possesses a nearly-native metallic surface, which allows the study of the effects of the behaviour of a small scale particle under the Gibbs-Thomson effect on the compaction process. The grain size evolution during compaction and the mechanical properties of the bulk components have been also been characterized. Micron scale powders were also consolidated for comparison purposes.

4.2. Experimental procedures

4.2.1 Starting Materials

Two different powders were used throughout this work: i) nano-Ag and ii) micro-Ag, used as a reference. The respective characteristics of the starting powders are shown in Table 4.1.

Table 4.1. Characteristics of the starting powders

| | Purity | Average Particle Size (APS) | Morphology | Supplier |
|-----------------|--------|--------------------------------|------------|--|
| <i>Nano-Ag</i> | 99.9% | 30-50 nm | spherical | Nanostructured & Amorphous Materials Inc |
| <i>Micro-Ag</i> | 99.9% | -325 mesh (<44 μm) | spherical | Alfa Aesar |

4.2.2 Consolidation Process

The shock compaction experiments were carried out at the Energetic Materials Research and Testing Center (EMRTC, Socorro, NM) according to their standard procedures [3.47]. The single tube set-up, where the explosives are in direct contact with the test tube, was used. This experimental arrangement was selected because the pressures applied on the powder bed are smaller than for the flyer tube assembly. The starting powders were cold pressed in a seamless powder container steel tube (12 mm inside diameter; 2.3mm of wall thickness) under a pressure of 325 MPa. The end plugs were welded using the tungsten inert gas welding process. The tests tubes were centered in a 15 cm diameter by 40 cm cardboard tube and subsequently filled with ANFO explosive (detonation velocity 2.6km/s). A sheet of C3 was used as the booster to initiate the detonation. Upon initiation of the explosive, a detonation wave propagated vertically downward, producing a calculated implosion pressure of ~1.5 GPa, which was transmitted to the powders. After the compaction, the enclosed containers were recovered and the Ag samples were extracted by machining the initial enclosed container.

4.2.3 Characterization of Consolidated Specimens

4.2.3.1 Density

Density was measured with a Gas Pycnometer (Micromeritics model AccuPyc 1330 Pycnometer). The reported values represent an average of 10 measurements.

4.2.3.2 Microstructure Analysis

The micron-scale materials were prepared using a standard metallographic procedure. The preparation of the specimens involved mounting them in bakelite followed by grinding and polishing them down to 0.02 μm diamond suspensions with an alcohol-based lubricant. The specimens were chemically etched (100 ml 95-98% H_2SO_4 and 2.5g CrO_3) to reveal the microstructure and were examined using a Nikon light optical microscope equipped with a Clemex Vision System. The same system was used to perform the image analysis of the various micrographs. A Hitachi S-4700 field emission gun scanning electron microscope (FE-SEM) was used to study the fracture surface of all specimens. Transmission electron microscopy (TEM) investigations were performed on a Hitachi H-9000 NAR, operating at 300 kV. Sample preparation was done by cryotomy. XRD patterns were acquired with a Philips PW1710 diffractometer using a monochromatized $\text{Cu K}\alpha$ radiation ($\lambda = 0.15405 \text{ nm}$). The full width at maximum height analysis was used to calculate the grain size and lattice microstrain from the broadening [4.4]. Annealed micron-scale powder was used as a reference to remove the instrumental broadening contribution.

4.2.3.3 Hardness Testing

Hardness was measured across the specimen diameter with a Clark Microhardness Tester (model CM-100AT) using a 200 g load. Each of the reported values represents an average of 3 indents.

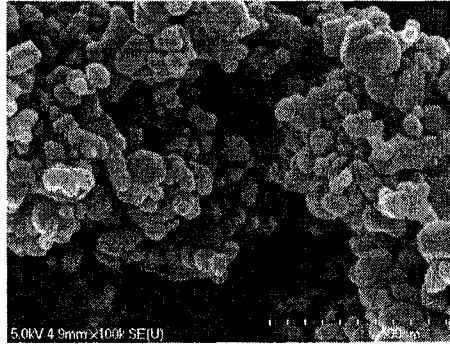
4.2.3.4 Compression Testing

Cubic specimens of 3x3x3mm were used for compression tests. The analysis of these specimens was performed on a Materials Testing System (MTS Model 810) machine equipped with a hydraulic actuator that generated the force and linear displacement. During compression testing, thin sheets of mica (50 to 80 μm thick), separated by a layer of boron nitride powder were placed between the face of the compression specimens and the anvils in order to maintain uniform deformation. The specimens were deformed at a strain rate 0.01/s up to fracture.

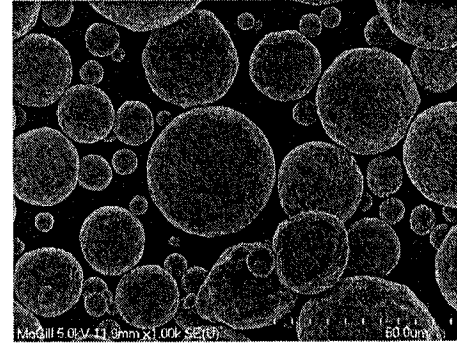
4.3. Results

4.3.1 Starting Materials

Figure 4.1 (a) shows the morphology of the nano -Ag starting powder. It can be seen that the particles have mostly a spherical morphology, with a narrow size distribution of ~30-50 nm. The micrographs validate the average particle size (APS) presented in Table 4.1. Figure 4.1(b) depicts the spherical morphology of the micron-scale powders.



(a)

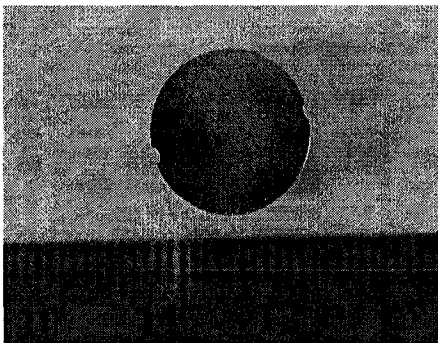


(b)

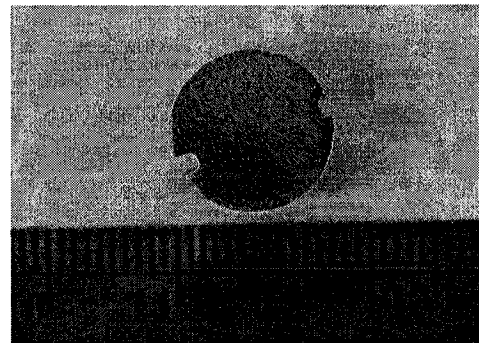
Figure 4.1. Scanning electron micrographs of two starting powders (a) nano-Ag powder, and (b) micro-Ag powder.

4.3.2 Macrostructure of Bars

After consolidation, the bulk samples had final dimensions of 12 mm in diameter and approximately 30 mm in length. Figures 4.2(a) and (b) show the cross section of the nano-Ag specimen and micro-Ag specimen, respectively. As depicted, no typical macro-scale defects, which are often observed in shock compacted samples, such as circumferential or transversal cracks or mach steam, were observed.



(a)



(b)

Figure 4.2. Cross section of the (a) nano-Ag specimen, and (b) micro-Ag specimen.

4.3.3 Density

The average density of the micro-Ag specimens was $9.6981 \pm 0.0289 \text{ g/cm}^3$, which corresponds to 92.5% of the theoretical density (TD) of silver. On the other hand, the nano-Ag specimen possessed an average density of $10.4425 \pm 0.0603 \text{ g/cm}^3$, which translates to 99.5% TD.

4.3.4 X-ray Diffraction

Figure 4.3 shows a collection of XRD patterns for the consolidated nano-Ag specimens, the bulk micro-Ag specimens and the starting nano- and micro-Ag powders, respectively. It can be seen that the consolidated process causes the XRD peaks to broaden slightly due to the nano-scale grain size and the creation of lattice strain. The respective grain sizes and lattice strains of the consolidated specimens and starting powders were calculated using the full width at maximum height and the numerical results are presented in Table 4.2. It can be remarked in that table that the calculated average particle size of the nano-scale powder using this technique is in agreement with the reported value from the manufacturer (see Table 4.1) and the micrograph presented in Figure 4.1(a). The average grain size of consolidated nano-Ag specimen was $56 \pm 5 \text{ nm}$ and the lattice strain was 0.22%. In comparison, the micron-scale samples show a significant increase in lattice strain caused by the intense plastic deformation of the process.

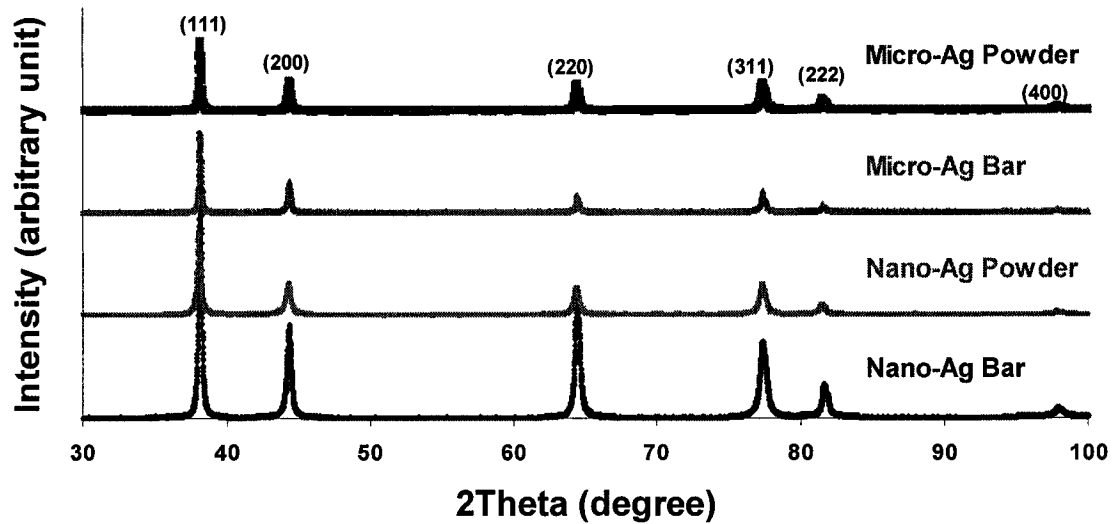


Figure 4.3. Collection of X-ray diffraction patterns from the consolidated nano-Ag specimen, micro-Ag specimen and the starting nano-Ag and micro-Ag powders, respectively.

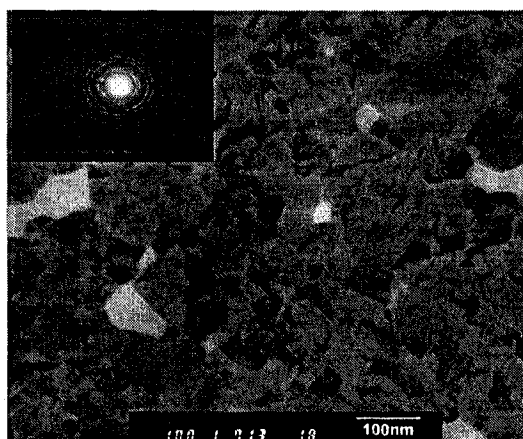
Table 4.2. Comparison of the average grain size and lattice strain of the consolidated bars and starting powders specimens.

| | Grain Size (nm) | Lattice Strain (%) |
|-----------------------|-----------------|--------------------|
| <i>Nano-Ag Powder</i> | 34±5 | N/A |
| <i>Nano-Ag Bar</i> | 56±5 | 0.22 |
| <i>Micro-Ag Bar</i> | N/A | 0.93 |

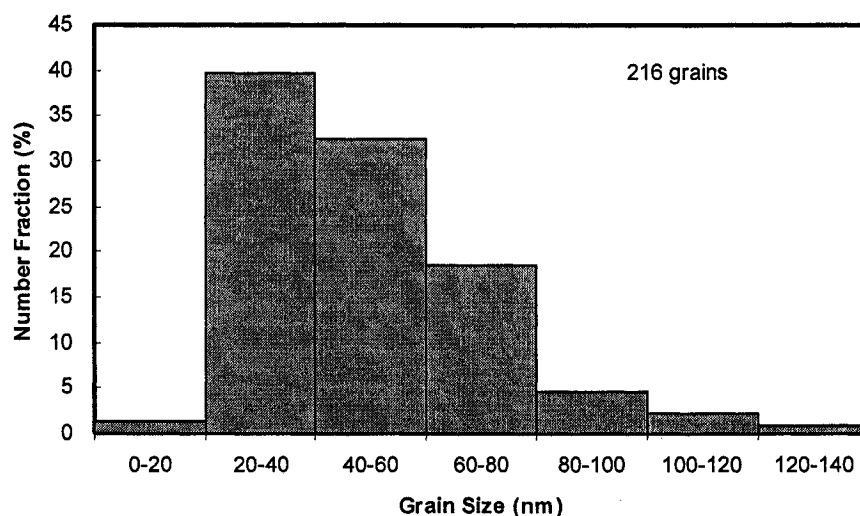
4.3.5 Microstructure

Figure 4.4(a) shows a typical TEM image of the center and side of the nano-Ag bar. Similar micrographs were obtained at the periphery of the samples. The spotted rings in the selected area diffraction pattern, illustrated in Figure 4.4(a), confirms the polycrystalline nature of the consolidated material. There is no

apparent evidence of melting of the silver particles from adiabatic heating during the compaction. Figure 4.4(b) displays the grain size distribution obtained by the average diameter method from the TEM micrographs, indicating an average grain size of $49 \pm 22 \text{ nm}$ in the consolidated samples. The average grain size is consistent with the grain size calculated from XRD line-broadening analysis.



(a)



(b)

Figure 4.4. (a) TEM bright-field image of nano-Ag specimen including selected area diffraction pattern and (b) grain size distribution measured from TEM images.

Figure 4.5 shows an optical micrograph of an etched specimen made out of micro-scale powder. The micrographs revealed that after consolidation, the shape of the particles changed from spherical to polygonal, as depicted in Figure 4.5 where the arrows are pointing at the particle boundary. The change in shape occurred from the material flow into the interparticle voids that were present prior to the consolidation process. Few voids are shown to be present at the triple junctions, indicating insufficient compaction energy to obtain pore-free samples. The observation of residual pores is in agreement with the density measurements obtained. The grain size range was between $5.27 \pm 2.00 \mu\text{m}$.

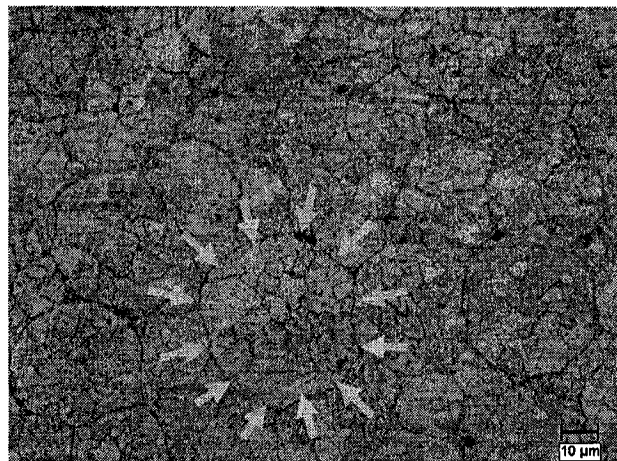


Figure 4.5. Optical micrograph of micro-Ag specimen

Mechanical properties

4.3.6 Hardness

The microhardness profiles through the diameter of the specimen are presented in Figure 4.6. In the case of the nano-Ag specimen, the average hardness was

83±1 HV. The profile shows no major variation in hardness across the diameter. For the micron-scale sample, the initial hardness of the micro-Ag powder (as starting material) was ~ 85 HV. When compared to the starting powder, the consolidation process increased the hardness of the consolidated bar by 33% (average of 113±10 HV in zone I). The increase in hardness can be explained by the strain hardening during the plastic deformation undergone by the Ag powders during consolidation, as previously shown in Figure 4.5. A drop in hardness is also observed near the center of the specimen. It is believed that recovery occurred in this zone due to the interaction of the concentric shock front. The average grain size in the zone possessing a reduced hardness was 6.01±1.91 mm, which is not significantly different than for the grains in the periphery, illustrating that the inside temperature was insufficient to cause recrystallisation.

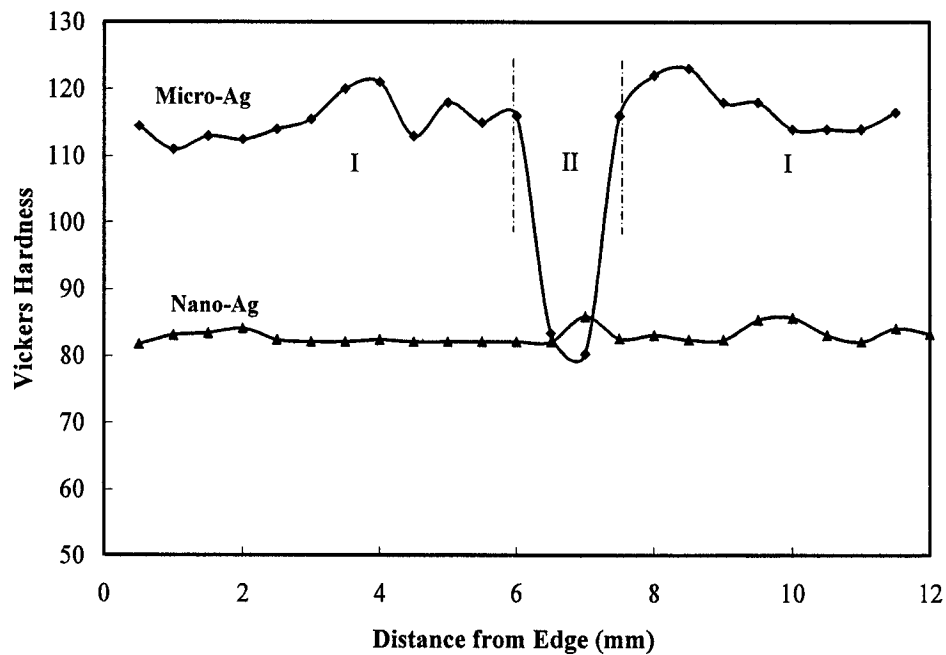


Figure 4.6. Microhardness of nano-Ag and micro-Ag specimens

4.3.7 Compression Testing

Figure 4.7 presents the compression stress strain curves obtained for nano-Ag and micro-Ag specimens for tests performed at a strain rate of 0.01/s and a summary of all mechanical properties is presented in Table 4.3. It can be seen that there is a significant difference between the flow behaviours of the nano - Ag and micro - Ag specimens, where the nano-Ag specimens exhibited a higher flow stress and good ductility. The nanostructured samples possessed an average compressive yield strength of 320 MPa, an average ultimate tensile strength of 390 MPa and an average strain fracture was 0.25. In comparison, the sample fabricated using the micron-scale powders exhibited a brittle behaviour with a strength level approaching 100 MPa.

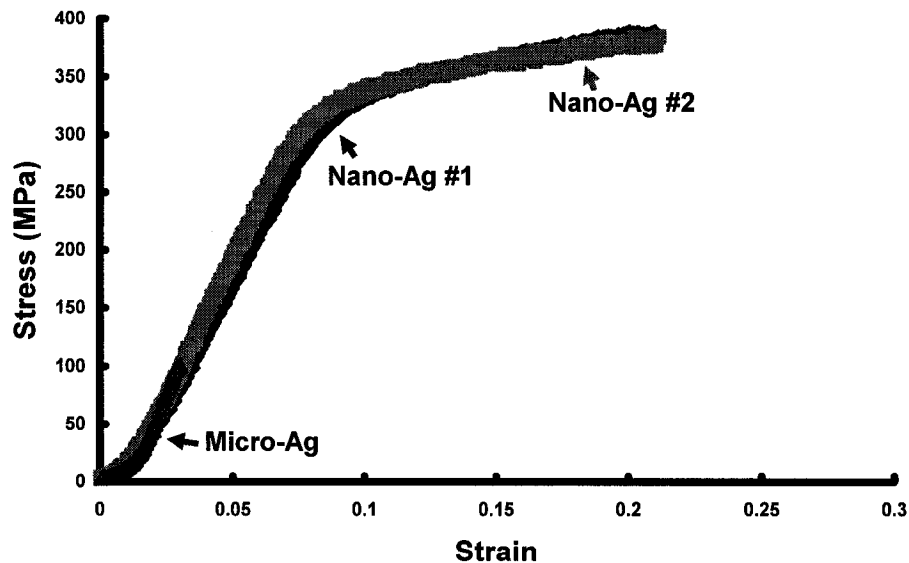


Figure 4.7. Stress-strain curves of nano-Ag and micro-Ag consolidated bars

Table 4.3. Comparison of the Mechanical Properties of nano-Ag and micro-Ag Specimens

| | GS | YS (MPa) | UTS (MPa) | EI (%) | Hardness (HV) |
|---------------------|-------------------|-------------|--------------|-----------|------------------|
| <i>Nano-Ag Bar</i> | ~60nm | 320±10 | 390±10 | 23±2 | 83±1 |
| <i>Micro-Ag Bar</i> | 5.27±2.00 μ m | 100 | 100 | 0 | 113±10 |

Figure 4.8 presents low and high magnification micrographs of the fracture surfaces.

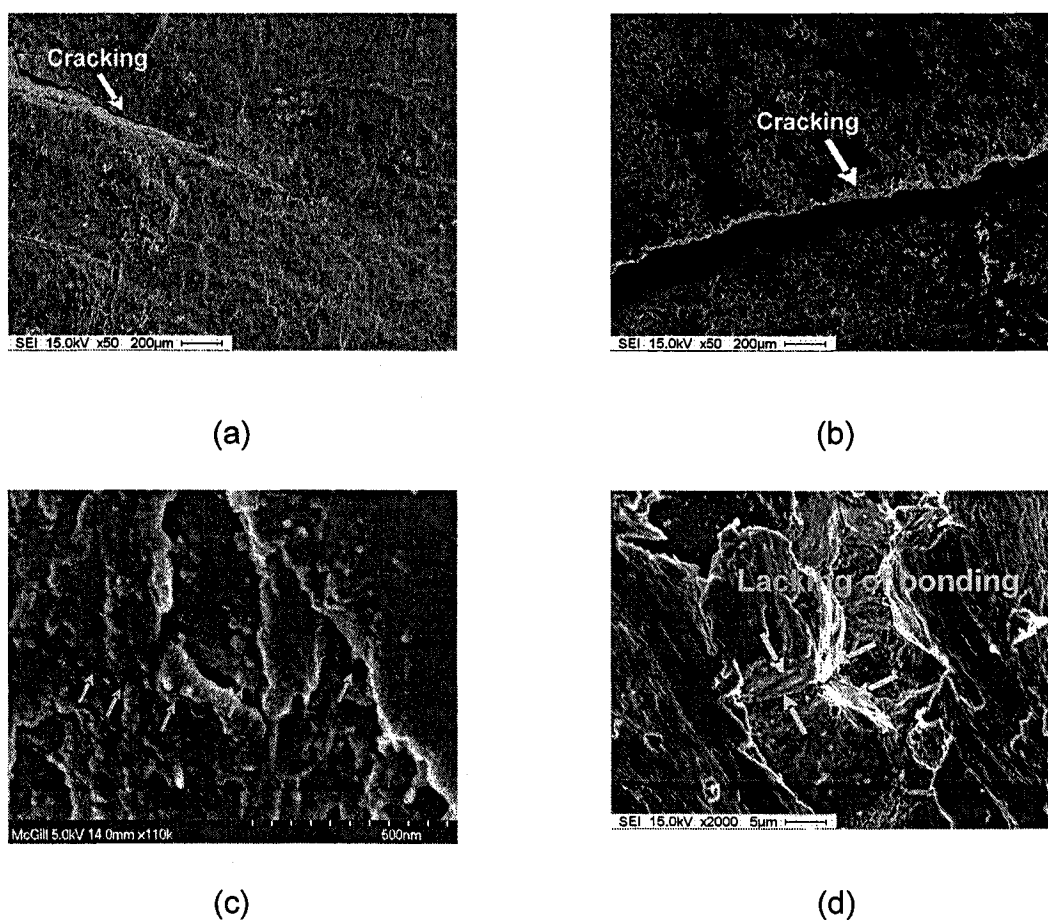


Figure 4.8. SEM of the broken specimens, with low magnification (a) nano -Ag, (b) micro -Ag, and with high magnification (c) nano -Ag, (d) micro -Ag.

No significant difference in the fracture surface was observed between both specimens at low magnification (see Figure 4.8(a) and (b)). However, at higher magnification, the fracture pattern was different. Figure 4.8(c) shows the surface fracture of the nano-Ag sample. No significant interparticle crack pattern or dimples was observed. On the other hand, Figure 4.8(d) shows clearly that the crack propagated along grain boundaries (arrow), for the micron-Ag samples. The intergranular aspect of the fracture surface is a sign of a lack of bonding between the original Ag particles, which also explains the low strength obtained.

4.4. Discussion

Several studies have shown that the densification of nano-sized powder is harder than for that of their micron-scale counterparts mostly because of the friction forces between particles and agglomeration problems [4.1]. For these reasons, the fabrication of nanostructured components using nanostructured powder as a starting material is sometimes preferred. On the other hand, the nano-sized powder has the advantage of a very high surface energy caused by the high surface area to volume ratio. In particular, several studies have shown that the melting temperature of nano-particles reduces nearly linearly with the inverse of the particle diameter [4.5]. It is also well known, under the Gibbs-Thomson effect, that nano-particles have a tendency to sinter or to Ostwald ripen, which reduces the total free energy of the system [4.6]. Jackschath et al [4.7] reported

that under the beam energy of a TEM (TEM vacuum level), coalescence of Ag clusters occurs spontaneously until the particle reaches a threshold diameter of 30nm, and where agglomeration rather than coalescence occurs for larger particles. During the coalescence stage, melting and formation of metallurgical bonds between particles occurs. The spontaneous coalescence to agglomeration transition explains why most commercially available Ag nanoparticles are available in an agglomerated form with average particle sizes of 30-50nm, like the ones used in this study. The results obtained in this study demonstrate that the formation of metallic bonds between the Ag particles of the aggregates is possible by solely applying a high pressure level. In terms of reactivity of nano-particles, the Ag particle has the advantage of being one of the more stable and is therefore less prone to having a surface oxide scale found, for example, on aluminum nano-particles. Nieh et al [3.2] studied the dynamic compaction of nano-Al crystal under pressure levels of 2-3 GPa and nearly fully dense compacts were obtained. However, TEM observations showed pores at the triple junctions, which were associated with the surface oxide layer that corresponded to approximately 20% of the diameter of the Al crystals. The presence of this oxide layer prevented the formation of metallurgical bonds, which was not the case in the present study.

There are seven agreed upon modes of energy dissipation performed by the powder bed in the shock compression of powders: void collapse energy, melting at the particle surface, defect energy, reaction bonding energy, fracture energy,

friction energy and microkinetic energy [3.48]. An evaluation of the contributing phenomena during the consolidation of the porous body is necessary in order to estimate the overall energy requirements of the shock pressure. Our results showed that a pressure level of ~2 GPa was sufficient to compact the porous bed and to form metallurgical bonds within an agglomerate of Ag nano-particles. The experimental results suggest that the shock energy was dissipated by void collapse since full dense compacts were obtained. In addition, friction energy to overcome the reported high friction force between nanoparticle displacement, microkinetic energy and possibly the formation of defects also may have contributed to the dissipation of the shock energy. These last criteria are difficult to evaluate since work hardening in nanomaterials possessing similar grain size is generally very low [1.11]. It is worth mentioning that because no evidence of melting between the different particles was observed on the TEM micrographs, we believe that the increase in temperature caused by the friction between the various particles was limited to negligible. The mechanism of particle-bonding is believed to be similar to the clustering effect observed in nanoparticles. Therefore, the combination of the oxide-free surface, the ultra-fine particle size (Gibbs-Thomson effect) and the intimate contact created by the pressure front is believed to have been sufficient to create metallurgical bonds throughout the compact. Similar pressures to the one used in this study were used to hot press Cu and Pd nano-powder fabricated by inert gas condensation [4.8]. The reported densities of bulk nanocrystalline materials consolidated under a pressure of 1.4 GPa in a heated die are 95.3-98.5% of TD for palladium, and 92.5-98.4% of TD

for Cu, respectively. Despite the fact that similar compaction pressure was used during hot pressing, a certain level of porosity remained in the samples and likely can be associated with possible contamination of the starting powder. In such cases the surface energy is lowered and insufficient coalescence of the nanoparticles occurs. Results by Ide [4.6] showed that under a pressure of 5 MPa and temperature of 300°C, Ag nanoparticles of 5 nm will self sinter to create a dense interlayer. This experimental evidence shows that both techniques are viable for fabricating nanomaterials from nano-powders. The advantage of shockwave compaction over the more conventional routes is the absence of a pressure gradient during compaction, while pressure gradients are common in any conventional pressing route. One can expect the possibility of fabricating larger-scale nanomaterials using dynamic consolidation. The rate at which the pressure is applied on the powder bed might also have an effect on the coalescence of the nanoparticles.

The presented results obtained for the micron powder were expected since the contribution of the surface energy of these powders is negligible compared to the total energy of the particle. Since no experimental results on the shockwave consolidation of Ag micron powders was found in the literature, the empirical relationship between the hardness and the shock pressure presented by Meyers and Thadani [4.9] was used to approximate the necessary compaction pressure. The results show that for a starting powder possessing a hardness of 85 HV, a required shock pressure of ~2.5-3 GPa is necessary to obtain well compacted

samples. Since the applied pressure was lower than the approximated pressure levels required for shock compaction of micron-scale powders, no strong bonds between the particles was created and an incomplete densification of the porous media was observed. In addition, the lack of bonding caused by the absence of surface melting, which is the known mechanism to achieve bonding between micron-scale particles [3.48], explains the very weak properties of the micron scale Ag samples. The reason for this explanation is that mechanical integrity is solely attributed to the mechanical interlocking between the particles. Results presented by Ide et al. [4.6] demonstrated that the contribution of the surface energy of particles of 100nm is insufficient to obtain a full density compact during low-temperature, low-pressure hot pressing and is in agreement with the results obtained in this study.

The nanostructure samples present an interesting combination of high strength and ductility, which is not available in wrought Ag material. Imposing a cold work level of 75% on commercial silver wires increases the ultimate tensile strength to 335 MPa but decreases the ductility level to nearly 0% [4.10]. For the same wire, in order to obtain ductility levels similar to those of the nanostructured materials used in this study, the wrought material must have a maximum tensile strength of 205 MPa [4.10]. The stress-strain curves presented in Figure 4.7 show an appreciable level of ductility without strain-hardening. The ductility in nanomaterials is function of the grain size, where numerous mechanisms significantly affect the ductility. Wadsworth and Nieh [4.11] reported that the Hall-

Petch relation would breakdown at a certain grain size (l_c), i.e. the critical grain size at which a dislocation pile-up will not be effective. From Eq. 4.1 and the following data (G: 30 GPa, b: 0.289 nm, ν : 0.39, and H: 0.814 GPa), the critical grain size at which the Hall-Petch relation will break down was calculated for Ag and a critical grain size of 16.7 nm was determined.

$$l_c = \frac{3Gb}{\pi(1-\nu)*H} \quad (\text{Eq. 4.1})$$

Since the measured average grain size for the shock consolidated sample is larger than the critical grain size (49 nm vs 16.7 nm), it is assumed that a dislocation pile-up will be effective for the nanostructured materials of this study. The literature shows that for these materials, the compressive yield strength of nanocrystalline materials is approximately equal to $HV/3$ [4.8, 4.12]. The results obtained in this study are in agreement with these values: compressive yield strength: 0.31 GPa and Vickers Hardness/3: 0.27 GPa. Nanomaterials are also known to possess an inverse proportionality between the yield strength and the elongation [3.94, 4.13]. Despite the fact that the plot consists of a compilation of results from tensile tests, the point corresponding to our compressive test results is in agreement with the yield strength/elongation relationship of other nanostructured systems. The flat compression curve obtained was also observed in other nanocrystalline systems [4.14, 4.15]. The absence of strain-hardening is caused by the room temperature dynamic recovery known to nanomaterials [1.11]. A steady state dislocation density was obtained by the competition of dislocation generation at the grain boundaries and the dislocation

annihilation at the grain boundaries (the boundaries act as a dislocation sink) during plastic deformation.

4.5. References

- [4.1] Groza J.R., Dowding R.J., Nanostructured Materials 1996;7:749
- [4.2] Han Y.S., Seong B.S., Lee C.H., Lee G.H., Rhee C.K., Kim W.W., Wiedenmann A., Physica B: Condensed Matter 2004;350:1015
- [4.3] Linse V.D., Dynamic compaction of metal and ceramic powders. In: edited by National Materials Advisory Board. NMAB-394. National Academy Press, Washington (DG): 1983. p. 1.
- [4.4] Klug H.P., Alexander L., X-ray diffraction procedures for polycrystalline and amorphous materials. New York (NY): John Wiley & Sons, 1974. p. 661.
- [4.5] Allen G.L., Bayes R.A., Gile W.W., Jesser W.A., Thin Solid Films 1986;144:297
- [4.6] Ide E., Angata S., Hirose A., Kobayashi K.F., Acta Materialia 2005;53:2385
- [4.7] Jackschath C., König L., Rabin I., Schulze W., Tesche B., Nanostructured materials 1993;3:181
- [4.8] Youngdahl C.J., Sanders P.G., Eastman J.A., Weertman J.R., Scripta Mater 1997;37:809
- [4.9] Meyers M.A., Thadhani N.N., Yu L.H., Explosive shock wave consolidation of metal and ceramic powders. In: Murr LE, editors. Shock Waves for Industrial Applications, Noyes (NJ): 1988. p. 265.
- [4.10] Metals Handbook, Ninth Edition, Volume 2; Properties and Selection: Nonferrous Alloys and Pure Metals, 1979, p.672

- [4.11] Nieh T.G., Wadsworth J., Scripta Metallurgica and Materialia 1991;25:955
- [4.12] Suryanarayana R., Frey C.A., Sastry S.M.L., Waller B.E., Buhro W.E., Processing and properties of nanocrystalline materials. In: Suryanarayana C, Singh J, Froes FH, editors. Warrendale, TMS, 1996.
- [4.13] Zhu Y.T., Liao X., Nature Mater 2004;4:351
- [4.14] Jia D., Wang Y.M., Ramesh K.T., Ma E., Zhu Y.T., Valiev R.Z., Appl Phys Lett 2001;79:611
- [4.15] Jia D., Ramesh K.T., Ma E., Scripta Mater 2000;42:73

CHAPTER 5

THE INFLUENCE OF SURFACE ROUGHNESS ON STRENGTH AND DUCTILITY OF SHOCKWAVE CONSOLIDATED BULK NANOSTRUCTURED SILVER

5.1. Introduction

The mechanical properties of nanomaterials vary significantly from those of their micron-scale counterparts. Several studies comparing characteristics such as hardness or tensile properties can be found in the literature and are summarized by Meyers et al. [1.11]. The relationship between an increase in strength and hardness at the expense of ductility is generally accepted by the materials science community [1.11]. However the review article by Meyers et al. [1.11] reported molecular dynamic simulations that were performed to try to explain the reduction in ductility observed. At the nanoscale, conventional deformation techniques based on dislocation and hardening have reduced efficiency because as the size of dislocation approaches grain size, grain boundary sliding and twinning is more likely to occur during the deformation process [1.11]. Despite

recent advances in deformation techniques, a process to effectively deform materials with a grain size between 10-100 nm has yet to be found although progress has been made in pursuit of this goal. Koch [5.1] has shown that artifacts from processing, such as pores and cracks, tensile instabilities and crack nucleation significantly contribute to the reduction in ductility in the resulting materials. In addition, Ma [3.95] reported eight approaches used to improve the ductility without significantly sacrificing the increased strength in nanomaterials. In that study, the fabrication of flawless materials figured among the proposed mechanisms. Ma et al. [3.108] have also produced flawless nanocrystalline copper using a proprietary in-situ consolidation, which possesses a strength level above 1100 MPa with a true strain of 0.15.

Conventional materials possessing high strength and high ductility also possess high fracture toughness. Thus, the lower ductility behavior for materials possessing a grain size between 10-100 nm would infer reduced toughness. Studies examining Charpy impact testing are currently emerging, but limited results on few systems are available. Stolyarov et al. [5.2] reported that for ultra fine grain (UFG) Ti prepared by Equal Channel Angular Pressing (ECAP), a 7-8% increase in toughness was observed in comparison to the conventional materials. Unfortunately, no grain size distribution was reported. Karimpoor et al. [3.113] reported a room temperature impact energy 4 times lower in electrodeposited nanocrystalline Co samples (grain size ~18 nm), as compared to the annealed micron-scale Co. In another study, Karimpoor et al. [3.114] reported a

comparison of tensile strength properties for nanocrystalline and polycrystalline Co. The results of that study show that despite a more than twofold increase in strength, (yield strength: 421 MPa vs. 972 MPa and UTS: 869 MPa vs 1820 MPa) a 50% reduction in ductility (12% vs. 6.5%) was observed. These results could be an indication of a connection between the stress-strain behaviour and the previously mentioned lower impact resistance reported by Karimpoor [3.113].

The emergence of defect-free fabrication processes, such as electrodeposition and in-situ consolidation, is raising other concerns. Since no internal defects are to be present in the bulk nanomaterials, how surface defects, such as poor surface finish or surface scratches caused by regular wear, will influence the fracture properties is an important question. In this paper, the relationship between room temperature tensile properties, surface roughness and fracture toughness for shock consolidated nanocrystalline Ag samples will be reported.

5.2. Experimental procedures

Bulk nanostructured Ag rods were fabricated using dynamic compaction of spherical nano-Ag powders (99.9% purity) possessing an average particle size of 30-50 nm. A similar shock consolidation procedure to the one previously presented by Brochu et al. was used [5.3]. After consolidation, bars 30 mm in length and 11.5 mm in diameter were recovered and the density was measured with a Gas Pycnometer (Micromeritics model AccuPyc 1330 Pycnometer).

The microstructure of the nano-Ag samples was examined by transmission electron microscopy (TEM) (Hitachi H-9000 NAR), operating at 300 kV. Sample preparation was done by cryotomy. A Hitachi S-4700 field emission gun scanning electron microscope (FE-SEM) was used to study the microstructure and fracture surface of all specimens.

The different surface finishes were obtained using various stages of grinding/polishing. Three surface conditions were investigated, specifically 600 grit, 800 grit and 3 μm diamond surface finishes. The roughness average (Ra) and root-mean-square average (Rq) were measured to determine surface roughness characteristics for each sample with a Dimension 3100 Scanning Probe Microscope (SPM) using contact mode. The scanned areas were 100 μm x 100 μm .

Shear punch testing is a small-specimen testing technique that enables the characterization of the flow behavior of the material, in particular: yield, ultimate tensile strength and ductility. A complete description of the procedure and analysis of the load/extension curve can be found in Wanjara et al. [5.4].

5.3. Results and Discussion

The consolidation process employed in this study resulted in defect-free samples. The consolidated bars examined possessed an average density of $10.4425 \pm 0.0603 \text{ g/cm}^3$, which is equivalent to 99.5-100% of the theoretical density (TD) of bulk silver. The density of bulk nanostructured materials is slightly lower than that of their micron-scale counterparts [5.5]. Therefore, the density measurements obtained confirm the integrity of the compacted sample, in particular the lack of defects, such as porosity. In addition, no cracks or pores were observed using scanning electron microscopy.

5.3.1. Microstructure

Figure 5.1 shows a typical TEM image of the nano-Ag bar with spotted rings in the selected area diffraction pattern. The spotted rings confirm the polycrystalline nature of the consolidated material. The microstructures are indicative of a uniform and narrow grain size distribution and the image analysis measurement indicates an average grain size $49 \pm 22 \text{ nm}$.

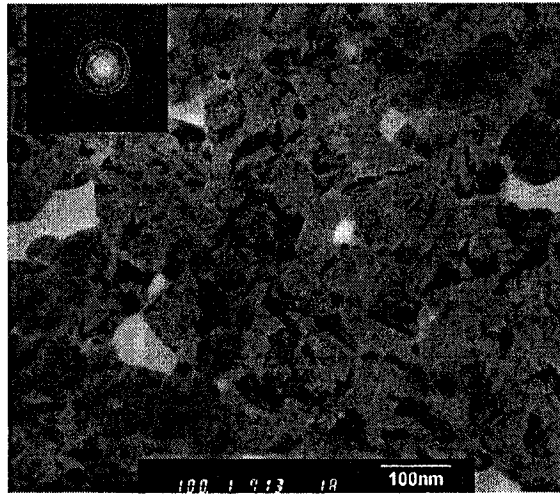


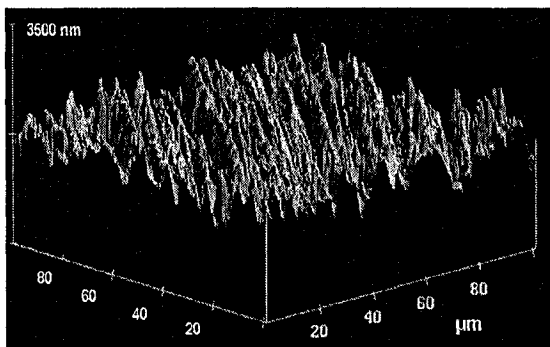
Figure 5.1. TEM bright-field image of nano-Ag specimen including selected area diffraction pattern

5.3.2. AFM

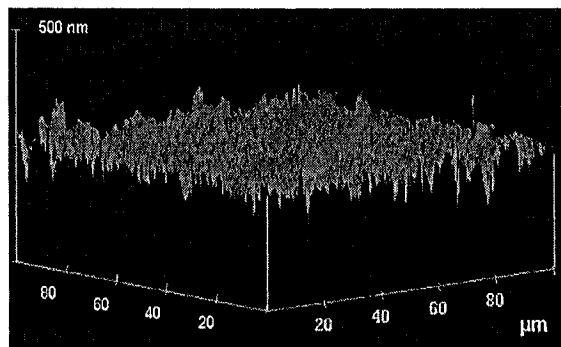
The measured values of roughness average (Ra) and root Mean Square Average (Rq) as a function of the last stage of grinding/polishing are presented in Table 5.1 and the corresponding 3-D AFM micrographs are presented in Figure 5.2. As shown, a significant difference in roughness was observed between the 600 grit surface finish and the finer 3 μm polishing stage. With respect to the grain size of the material, the grooves left from the 600 grit paper were several times deeper than the average diameter of the nanograin, while the asperities remaining after the polishing stage were smaller than the average grain. From this point on, roughness average values will be used to identify the different surface finishes.

Table 5.1. Values of roughness average (Ra) and root Mean Square Average (Rq) as a function of surface finish.

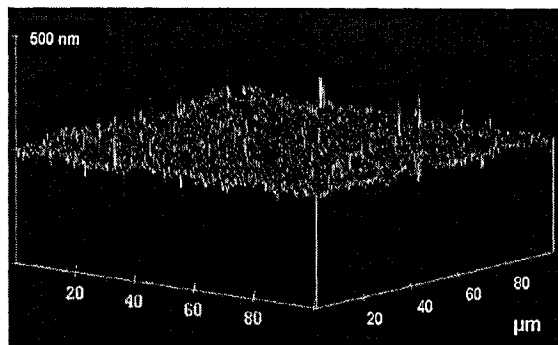
| Final grinding stage | Roughness average (Ra) | Root Mean Square (Rq) |
|------------------------------|---------------------------|--------------------------|
| 600 grit SiC | 266.7 ± 90 nm | 340.3 ± 100 nm |
| 800 grit SiC | 30.3 ± 0.7 nm | 40.2 ± 1.2 nm |
| 3 μ m diamond suspension | 12.1 ± 1.3 nm | 16.8 ± 0.7 nm |



(a)



(b)



(c)

Figure 5.2. AFM micrograph of sample with (a) 600 grit, (b) 800 grit and (c) 3 μ m surface finish.

5.3.3. Shear Punch Testing

The homogeneity of the mechanical responses of the nano-Ag samples after multiple tests is illustrated by the superimposition of the load-displacement curves in Figure 5.3, which were acquired using the shear punch testing method. The four samples presented had a roughness average of 30.3 nm. No significant strain hardening was observed for any of the samples, which is in agreement with tensile results obtained for other nanomaterials [5.1, 5.6, 5.7]. Comparable reproducibility in the load-displacement curves was observed for the other surface finishes that were tested. The samples exhibited the same mechanical responses for a particular surface finish which were independent from the area the samples were taken from in the consolidated bar. These results indicate the degree of consistency in the material where a direct correlation was observed between the surface roughness and strength as well as ductility.

Figure 5.4 shows representative load-displacement curves acquired for the three surface roughness stages studied. A drastic change in load-displacement behavior can be observed between the samples with a roughness average of 267 nm compared with the samples possessing roughness averages of 30 and 12 nm, respectively. The rougher samples exhibited a brittle behavior while the samples possessing a smoother surface displayed a certain level of ductility. A summary of the converted yield, ultimate tensile strength (UTS) and ductility as a function of the surface roughness is presented in Figure 5.5. The samples

possessing a surface roughness of 267 nm exhibited no plasticity and a fracture strength of 200 MPa. However, a reduction in the roughness to 30 and 12 nm, respectively, led to an increase in strength to 300-310 MPa and caused the appearance of plastic behavior ranging between 12-15%. The rougher surface therefore resulted in a 35% reduction in strength and a complete disappearance in ductility in comparison to the smoother samples. In addition, no statistical distinction between yield strength and UTS could be made as no significant work hardening was observed for the samples exhibiting ductility. Similarly, no statistical difference in ductility was observed for the samples with a roughness of 30 and 12 nm. By comparison, polycrystalline Ag possesses yield strength of 76 MPa, UTS of 140 MPa and elongation of 50% [4.10].

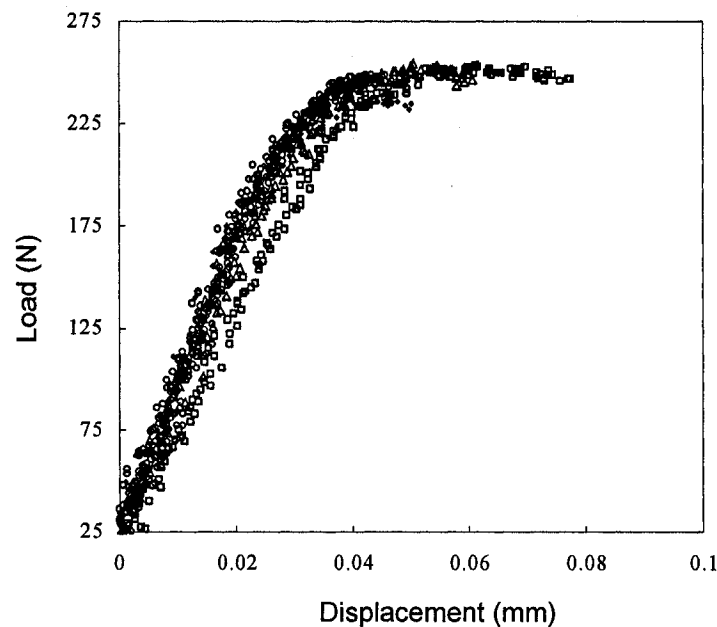


Figure 5.3. Load-displacement curves for samples possessing a roughness average of 30 nm.

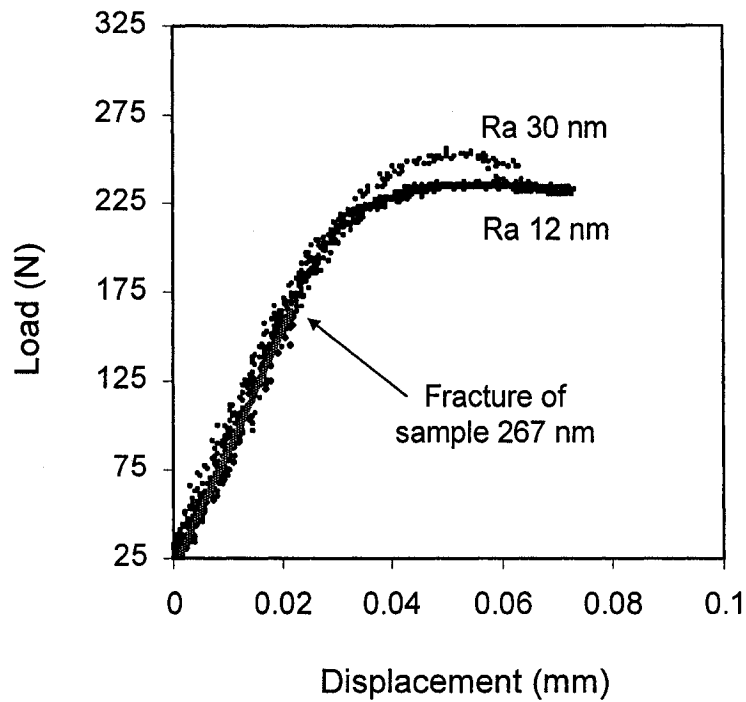


Figure 5.4. Comparison of the load-displacement curves for samples possessing roughness averages of 267, 30 and 12 nm, respectively.

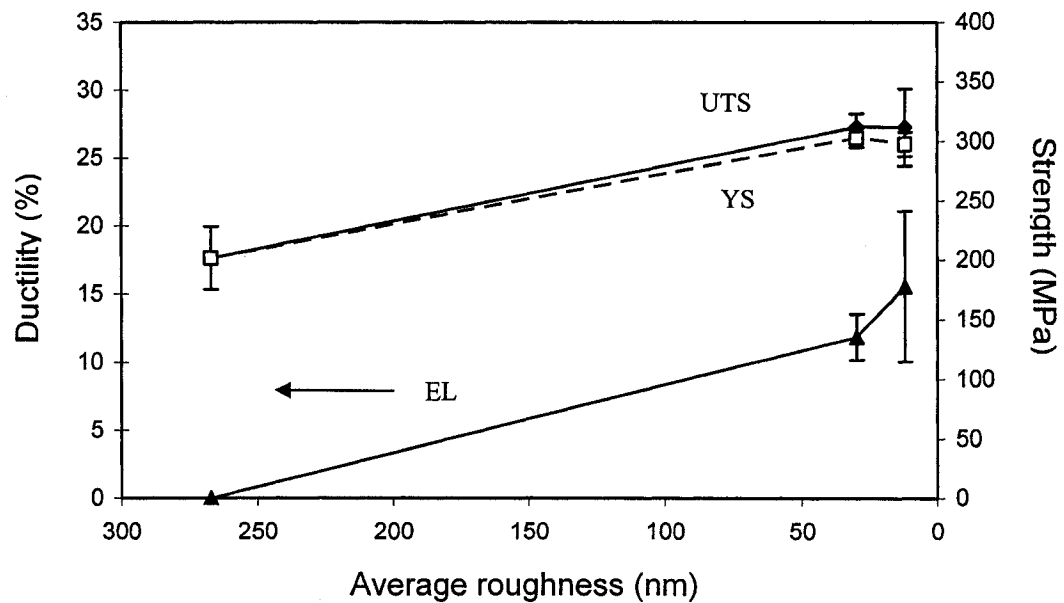
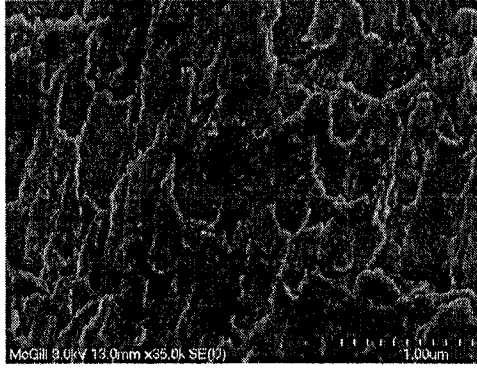


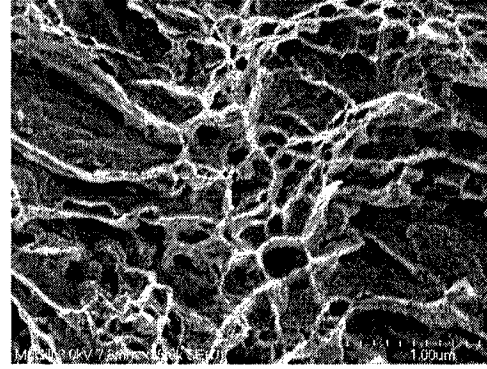
Figure 5.5. Comparison of strength (UTS and yield strength (YS)) and EL of shear punch testing as a function of surface finish.

5.3.4. SEM of Fracture Surface

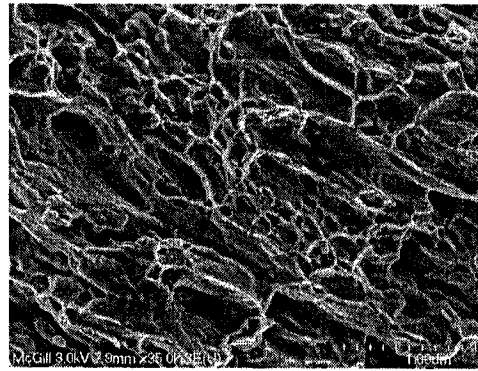
In an attempt to explain the primary difference in ductility observed during the shear punch tests, close analysis of the fracture surface was carried out. Figure 5.6 presents the fracture surfaces for (a) 267 nm, (b) 30 nm and (c) 12 nm surface finishes, respectively. A significant difference in the morphology of the fracture can be seen between the samples with no ductility and the other samples. This change in fracture morphology correlates with the level of ductility observed. The fracture surface of the samples exhibiting no ductility shows a morphology resembling intergranular fracture, where some of the curvature fits with the pull-out of a single grain. On the other hand, dimples were observed for the samples exhibiting ductile behavior. Xiao et al. [5.8] and Mirshams et al. [5.9] have observed similar morphology and have classified the fracture as being transgranular ductile. For both ductile fracture surfaces, the sizes of the dimples, which range from 100nm to 2-3 microns, are larger than the grain size of 49 ± 22 nm. Since dimples are formed from internal defects, the mechanisms responsible for void initiation in flawless materials are: existing voids at grain boundaries and triple points, voids created by dislocation emission from grain boundaries, voids created by grain-boundary sliding which leaves wedges at triple junctions and cavities created by the action of grain boundary sliding on the ledges [5.10]. The size of the dimples is a function of the spacing between the created initiation sites. The wide distribution of dimple size in the ductile samples suggests a non-uniform distribution of the site of initiation.



(a)



(b)



(c)

Figure 5.6. SEM of fracture Surface for (a) 267 nm, (b) 30 nm and (c) 12 nm surface finishes, respectively.

To quantify the fracture resistance of the bulk Ag nanomaterials, a classical fracture mechanics approach was used to calculate fracture toughness (K_{Ic}) from the critical stress (σ_f) for crack propagation and critical crack length (a_c) (Eq.5.1). The critical stress considered was the fracture strength obtained during the shear punch experiments and the critical crack length used was that of the surface roughness, as the theory that the material was flawless was assumed.

$$K_{Ic} = Y\sigma_f (\pi a_c)^{1/2} \quad (\text{Eq.5.1})$$

The shape factor (Y) of the crack was 1.1, which presumes that the defect causing the catastrophic fractures of the material was due solely to the surface roughness. In this calculation, the critical crack length (a_c) was assumed to be the roughness average and the calculated fracture toughness of bulk nanostructured Ag was found to be $0.2 \text{ MPa}\sqrt{\text{m}}$. By performing back-calculations, the critical fracture strength for the materials with a critical crack length of 30 nm and 12 nm was shown to be above the fracture strength measured, which indicates that ductility would be observed prior to catastrophic fracture and is thus in agreement with our aforementioned observations. The low fracture toughness detected conforms to empirical observations of the strong association between the strength and ductility and the presence of flaws [1.11]. Because no fracture toughness values for nanomaterials are available in the literature, no comparison can be made to previous studies. However, if fracture toughness is as low in other systems, this would correlate with the low Charpy impact results for nanocrystalline Co reported by Karimpoor et al. [3.113]. It is worth mentioning that Karimpoor reported dimples on the fracture surface, indicating plasticity despite the low impact strength.

5.4. References

[5.1] Koch C.C., *Nanocryst Mater* 2003;18:9.

[5.2] Stolyarov V., Valiev R.Z., Zhu Y.T., *Appl. Phys. Lett.*, 88, 2006, 041905.

[5.3] Brochu M., Zimmerly T., Ajdelsztajn L., Lavernia E.J., Kim G., Materials Science and Engineering: A, In Press, Corrected Proof, Available online 16 February 2007.

[5.4] Wanjara P., Brochu M., Jahazi M., Materials & Design, In Press, Corrected Proof, Available online 7 November 2006.

[5.5] Suryanarayana C., Intl Mat R 1995;40:41–64.

[5.6] Swygenhoven H.V., Caro A., Nanostruct Mater 1997;9:669–72.

[5.7] Carsley J.E., Fisher A., Milligan W.W., Aifantis E.C., Metall Mater Trans A—Phys Metall Mater Sci 1998;29:2261–71.

[5.8] Xiao C., Mirshams R.A., Whang S.H., Yin W.M., Mater Sci Eng A 2001;301:35.

[5.9] Mirshams R.A., Xioa C.H., Whang S.H., Yin W.M., Mater Sci Eng A 2001;315:21.

[5.10] Kumar K.S., Suresh S., Chisholm M.F., Horton J.A., Wang P., Acta Mater 2003;51:387.

CHAPTER 6

GENERAL DISCUSSION

The two manuscripts present the results from projects investigating the fabrication and the characterization of shock consolidated bulk nanostructured silver components from nano-sized powder. Primarily, the work focuses on the grain size evolution during consolidation, the mechanical properties of the bulk components, and the effect of surface finish on the mechanical and fracture behavior.

The nano-sized powders possess a very high surface energy caused by the high surface area/volume ratio, which is large advantage when attempting to improve consolidation [4.5]. An example of this high surface energy is the drastically reduced melting point attributed to nanoparticles in comparison to their micron-scale counterparts. In addition, small particles have greater vapor pressure, caused by their high radius of curvature, called the Gibbs-Thomson effect [4.6]. The Gibbs-Thomson effect is known to favor the bonding and coalescence of fine nanoparticles until the critical particle diameter is obtained. At this critical diameter, the driving force rising from the high vapor pressure is insufficient to allow self-sintering, which results in agglomeration. Another notable example of

the Gibbs-Thomson effect is Ostwald ripening, in which concentration gradients cause small precipitates to dissolve and larger ones to grow.

The results presented in this thesis show that a pressure level of 1.9-2 GPa applied on nanoparticles at room temperature is sufficient to generate metallurgical bonds within the compacted body of a sample and consolidation of the nano-Ag powders occurs at the same time. However, the pressure level required to create metallurgical bonds and consolidation in nanomaterials is lower than the necessary pressure to consolidate micron-scale materials where only future compaction was observed. Empirical analysis performed by Meyers et al. [3.48] showed that for a powder possessing a hardness of 85 HV, a shock pressure of ~2.5-3 GPa is necessary to fully consolidate the porous body. The lack of consolidation of the micro samples suggests that the applied pressure is lower than the required pressure for the consolidation of micron-scale powders. As presented in chapter 4, no strong bonds between the particles were formed and an incomplete densification of the porous body was observed.

Nieh et al [3.2] investigated the shock-compaction of aluminum nanocrystals possessing an average particle size of about 50-70 nm, under pressure levels of 2-3 GPa. After consolidation, the average grain size ranged between 80-200 nm and almost fully dense compacts were obtained. However, TEM observations showed pores at the triple junctions and incomplete bonding between particles, which was associated with the presence of the oxide layer at the surface of the

particle. The oxide layer corresponded to approximately 20% of the diameter of the Al crystals. It is the presence of this oxide layer that prevents the formation of metallurgical bonds between particles. In this work, no significant oxide layer was present on the Ag nano powders, thus consolidation was permitted and defect free samples were created.

The ductility of nanomaterials is a function of the grain size, as mechanisms for plastic deformation are always a function of grain size. In the conventional grain size regime it is usual for a reduction in grain size to result in an increase in ductility, therefore one should expect a ductility increase as the grain size is reduced to nanoscale. Figure 6.1 illustrates normalized yield strength versus percentage elongation for metals with grain sizes in the nanocrystalline range [3.94]. There is a clear reduction in ductility as strength is increased. In order for nanostructured materials to be used for structural applications, processes where no reduction in ductility will occur when strength is increased need to be developed. Superposing the results obtained in this study on Figure 6.1 demonstrates that the nano-Ag obtained from the shockwave consolidation process presents an interesting combination of high strength and ductility, and thus is a step forward in the creation of structural applications.

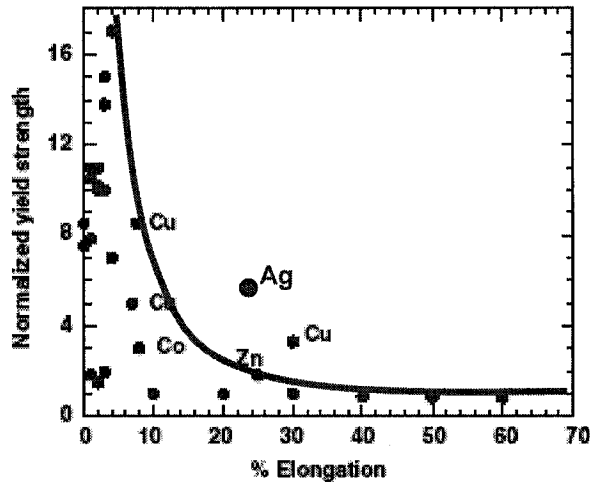


Figure 6.1. Compilation of yield stress versus % elongation of nanocrystalline metals [3.94].

The shear punch testing results indicate that there was a degree of consistency in the material, where a direct correlation was observed between the surface roughness and strength as well as ductility. The rougher samples exhibited a brittle behaviour as well as a reduction in strength and ductility. In comparison, the samples possessing a smoother surface displayed a certain level of ductility. The results reporting the effects of surface finish on the mechanical behaviour of shock consolidated nano-Ag demonstrate a strong connection between the presence of flaws and mechanical behavior. The fracture toughness measured for the nano-Ag samples ($0.2 \text{ MPa}\sqrt{\text{m}}$) is a strong indication of the influence of defects on the fracture behaviour of the material.

The major goal of this project was to fabricate nanostructured components from nano powder, with moderate applied pressure, in order to take advantage of the Gibbs-Thomson effect. The long-term goal is to produce bulk materials from

nano-powders in order to exploit the Gibbs-Thomson effect. In this initial project, silver was selected because of the nearly native metallic surface and relatively low cost compared to noble metals such as gold and platinum. Since this first step is a success, future work will be directed at shock consolidation of Cu, Ni, and Fe.

CHAPTER 7

SUMMARY

- Full dense bulk nanostructured silver components were fabricated from nano-size powder using a shockwave consolidation technique, and the samples demonstrate a strong connection between the presence of flaws and mechanical behavior.
- The average grain size is 49 ± 22 nm, which remained in the nanometer range.
- The average hardness of the bulk nanostructured component is 83 ± 1 HV.
- Compression results show strength of 390 ± 10 MPa, and ductility of $23\pm 2\%$, which is well above strength level obtainable from strain hardened Ag components.
- The fracture toughness calculated is $0.2 \text{ MPa} \sqrt{\text{m}}$, which indicates a strong correlation between defects and fracture toughness.
- The surface finish alone can inhibit plastic deformation and consequently, surface finish or surface wear will have to be carefully controlled to avoid catastrophic failure in the use of bulk nanomaterials in structural applications.